





ARTICLE

Determination of Tr1 cell populations correlating with distinct activation states in acute IAV infection

Caitlin A Abbott ^{1,✉}, Emily L Freimayer ¹, Timona S Tyllis¹, Todd S Norton¹, Mohammed Alsharifi ², Aaron H S Heng¹, Stephen M Pederson^{3,4}, Zhipeng Qu⁵, Mark Armstrong³, Geoffrey R Hill^{6,7}, Shaun R McColl^{1,†} and Iain Comerford ^{1,†,✉}

© 2023 Published by Elsevier Inc. on behalf of Society for Mucosal Immunology.

This is an open access article under the CC BY-NC-ND license (<http://creativecommons.org/licenses/by-nc-nd/4.0/>).

Type I regulatory (Tr1) cells are defined as FOXP3⁻IL-10-secreting clusters of differentiation (CD4⁺) T cells that contribute to immune suppression and typically express the markers LAG-3 and CD49b and other co-inhibitory receptors. These cells have not been studied in detail in the context of the resolution of acute infection in the lung. Here, we identify FOXP3⁻ interleukin (IL)-10⁺ CD4⁺ T cells transiently accumulating in the lung parenchyma during resolution of the response to sublethal influenza A virus (IAV) infection in mice. These cells were dependent on IL-27R α , which was required for timely recovery from IAV-induced weight loss. LAG-3 and CD49b were not generally co-expressed by FOXP3⁻ IL-10⁺ CD4⁺ T cells in this model and four populations of these cells based on LAG-3 and CD49b co-expression were apparent [LAG-3⁻CD49b⁻ (double negative), LAG-3⁻CD49b⁺ (double positive), LAG-3⁺CD49b⁻ (LAG-3⁺), LAG-3⁺CD49b⁺ (CD49b⁺)]. However, each population exhibited suppressive potential consistent with the definition of Tr1 cells. Notably, differences between these populations of Tr1 cells were apparent including differential dependence on IL-10 to mediate suppression and expression of markers indicative of different activation states and terminal differentiation. Sort-transfer experiments indicated that LAG-3⁺ Tr1 cells exhibited the capacity to convert to double negative and double positive Tr1 cells, indicative of plasticity between these populations. Together, these data determine the features and suppressive potential of Tr1 cells in the resolution of IAV infection and identify four populations delineated by LAG-3 and CD49b, which likely correspond to different Tr1 cell activation states.

Mucosal Immunology (2023) 16:606–623; <https://doi.org/10.1016/j.mucimm.2023.06.003>

INTRODUCTION

Respiratory infections caused by pathogens such as influenza A virus (IAV) and SARS-CoV2 are a cause of significant morbidity and mortality worldwide. Understanding how immune activation and suppression are balanced during acute respiratory infection is critical for developing effective therapeutic interventions to promote rapid tissue recovery while ensuring pathogen clearance. Antigen-specific immune suppression mediated by regulatory T cells (Tregs) plays an important role in control of the immune response, both in terms of its magnitude and resolution. FOXP3⁺ Tregs are the best-characterized T-cell population involved in regulation of the adaptive immune response to IAV, having been shown to permit establishment of appropriate protective responses^{1,2}, constrain pathological effector T-cell responses^{3–7}, and promote tissue repair⁸. However, other Treg subsets may also make important contributions during acute infection.

Type I regulatory (Tr1) cells were first described as interleukin (IL)-10-secreting clusters of differentiation (CD4⁺) T cells with a suppressive function that often co-express the T helper (Th)1 cytokine

interferon (IFN) γ ^{9–17}. However, current classification of this subset has been refined to exclude other subsets of CD4⁺ T cells that have the capacity to secrete IL-10, such as Tregs, Th2, Th3, Th9, Th17, and other T cells that lack suppressive functionality. Specifically, Tr1 cells are now generally accepted to be CD4⁺ T cells that do not express FOXP3 or produce cytokines associated with Th2 or Th17 cells and that suppress bystander T-cell activation^{10,11,18}. These cells develop in an IL-27-dependent manner from naïve precursors *in vitro*^{11,19–21} and can also emerge from other T helper lineages during adaptive immune responses *in vivo* in settings of chronic inflammation²². The suppressive activity of Tr1 cells is predominantly due to their production of IL-10 and expression of co-inhibitory receptors^{23–25}. Indeed, co-expression of one specific co-inhibitory receptor lymphocyte activation gene-3 (LAG-3) and an adhesion molecule (CD49b) have been shown to reproducibly identify Tr1 cells in both humans and mice during chronic inflammation and lethal infection^{23,26,27}.

Tr1 cells have been shown to inhibit pathogen clearance in models of chronic infection^{12,13,28} and these cells also dampen

¹The Chemokine Biology Laboratory, School of Biological Sciences, University of Adelaide, Adelaide, Australia. ²Research Centre for Infectious Diseases, Department of Molecular and Biomedical Sciences, University of Adelaide, Adelaide, Australia. ³Bioinformatics Hub, School of Biological Sciences, University of Adelaide, Adelaide, Australia. ⁴Black Ochre Data Laboratories, Indigenous Genomics, Telethon Kids Institute, Adelaide, Australia. ⁵School of Biological Sciences, University of Adelaide, Adelaide, Australia. ⁶Translational Science and Therapeutics Division, Fred Hutchinson Cancer Center, Seattle, USA. ⁷Division of Medical Oncology, University of Washington, Seattle, USA. ✉ email: caitlin.abbott@adelaide.edu.au < iain.comerford@adelaide.edu.au

immune responses during allograft survival and in autoimmunity^{20,27,29–31}. Although IL-10-producing T cells have been previously detected in acute infection settings^{32–39}, a precise investigation of Tr1 cells in this context using the currently accepted Tr1 cell classification criteria and using gold standard methods for detection of these cells has not been performed to date. Therefore we conducted a comprehensive assessment of Tr1 cells in IAV infection utilizing FOXP3^{RFP}IL-10^{GFP} dual reporter mice^{40,41} and carefully assessed cellular phenotypes and suppressive capabilities.

RESULTS

FOXP3⁻IL-10⁺ CD4⁺ T cells emerge during acute viral infection and this correlates with the resolution of the response

The significance of FOXP3⁻IL-10⁺ CD4⁺ T cells present in the lungs during the resolution of acute viral infection is not well understood. To address this, we utilized intranasal (i.n.) installation of X-31 H3N2 IAV. In C57Bl/6 mice, this infection leads to transient viral replication in the lungs associated with moderate weight loss that completely resolves by day 10 post-infection

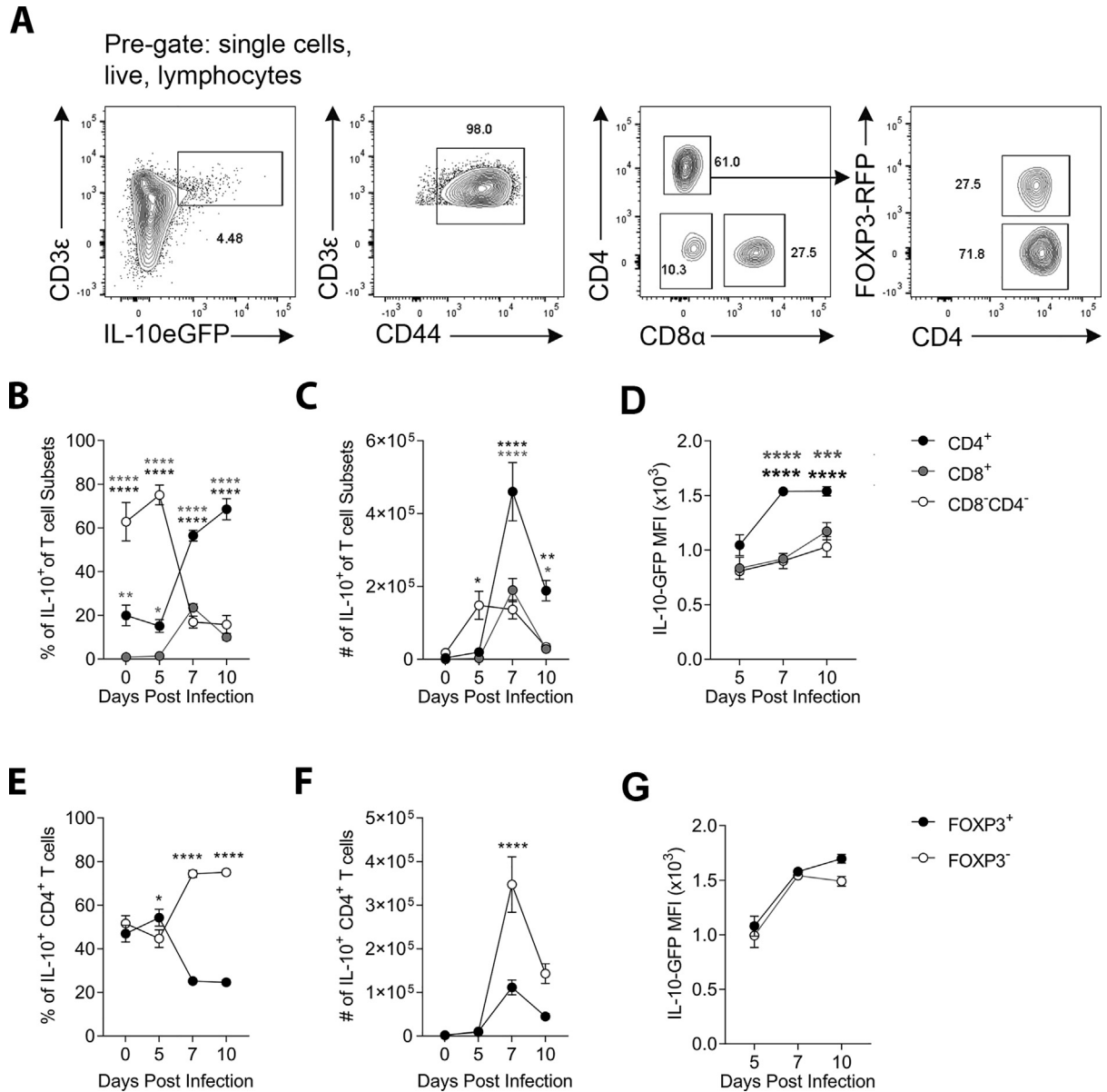


Fig. 1 FOXP3⁻CD4⁺ T-cells are the dominant source of T-cell-derived IL-10 during IAV infection. FOXP3^{RFP}IL-10^{GFP} mice were infected with X-31 IAV-intranasally and activated T-cell populations from the lungs were analyzed at days 0, 5, 7, and 10 post-infection. (A) Representative gating for identification of IL-10⁺ CD3⁺ T-cell populations from IAV-infected lungs. (B) Frequency, (C) number, and (D) MFI of IL-10-secreting CD8⁺, CD4⁺, and CD8⁻CD4⁻ T-cells. (E) Frequency, (F) number, and (G) MFI of IL-10-producing FOXP3⁻ (FOXP3⁻IL-10⁺ CD4⁺ T-cells) and FOXP3⁺ (regulatory T cells) over the course of IAV infection. (B, C, E, F) The mean is shown ± standard error of mean, $n = 7$ (day 0), $n = 9$ (day 5), $n = 13$ (day 7), $n = 10$ (day 10) biological replicates total from three independent experiments. Statistical analysis using one-way analysis of variance with Bonferroni's post-test. (D, G) The mean is shown ± standard error of mean, $n = 6$ (day 5), $n = 7$ (day 7), $n = 7$ (day 10) biological replicates total from three independent experiments. Statistical analysis using two-way analysis of variance with Bonferroni's post-test * $p \leq 0.05$, ** $p \leq 0.01$, *** $p \leq 0.001$, **** $p \leq 0.0001$. CD = clusters of differentiation; GFP = green fluorescent protein; IAV = influenza A virus; IL = interleukin; MFI = mean fluorescence intensity; RFP = red fluorescent protein.

(Supplementary Fig. S1). T cells that secrete IL-10 in the lung in this setting were identified and assessed by flow cytometry using FOXP3-RFP mice⁴⁰ crossed to IL-10-GFP (TIGER)⁴¹ mice, referred to hereafter as FOXP3^{RFP}IL-10^{GFP} mice (Fig. 1A). Prior to infection, and at day 5 post-infection, the majority of T-cell-derived IL-10 in lungs emanated from innate-like (CD4⁻CD8⁻) cellular sources (Fig. 1B and 1C). However, by day 7, CD4⁺ T cells were clearly the major T-cell subset responsible for IL-10 production, outnumbering IL-10⁺ CD8⁺ T cells approximately 2:1 (Fig. 1C) and producing significantly more IL-10 than other T cells in the lung on a per cell basis by mean fluorescence intensity (MFI) (Fig. 1D). Although there was some contribution from Tregs, defined here as CD4⁺ FOXP3⁺, to IL-10 production, the predominant CD4⁺ T-cell subset in the lung producing IL-10 was FOXP3⁻, consistent with a Tr1-like phenotype (Fig. 1E–G). These cells did not express *Il4*, *Il17a*, *Il22*, or *Csf1* but did express *Ifng*, *Tgfb*, and *Il21* (Supplementary Fig. S2), features that are in line with a Tr1-like cytokine signature^{10,27}.

To establish the kinetics of CD4⁺ T-cell accumulation during IAV infection, the abundance of activated effector cells (CD44⁺FOXP3⁻IL-10⁻), Tregs (CD44⁺FOXP3⁺IL-10⁻), IL-10⁺ Tregs (CD44⁺FOXP3⁺IL-10⁺), and FOXP3⁻IL-10⁺ CD4⁺ T cells (CD44⁺FOXP3⁻IL-10⁺) were quantified during the course of infection in the spleen, lung-draining mediastinal lymph node (mLN), lungs, and peripheral blood (Fig. 2). As expected, activated CD4⁺ effector T cells were the most abundant of these populations in each of the different compartments (Fig. 2A–E). In order to interrogate the differences in accumulation between the different Treg cell

populations (Tregs, IL-10⁺ Tregs, and FOXP3⁻IL-10⁺ CD4⁺ T cells) these populations were directly compared (Fig. 2A–E). This revealed that Tregs increased in the mLN and spleen between day 5 and 7 post-infection, however, this was not observed for FOXP3⁻IL-10⁺ CD4⁺ T cells or IL-10⁺ Tregs (Fig. 2A–C). However, both Tregs and FOXP3⁻IL-10⁺ CD4⁺ T cells had accumulated to a similar extent by day 7 in the lungs (Fig. 2A and 2D). In addition, compared to Tregs, neither FOXP3⁻IL-10⁺ CD4⁺ T cells nor IL-10⁺ Tregs substantially increased in frequency in the blood (Fig. 2A and 2E). Together, these findings are consistent with limited generation of FOXP3⁻IL-10⁺ CD4⁺ T cells and IL-10⁺ Tregs in secondary lymphoid organs and instead support the notion that both FOXP3⁻IL-10⁺ CD4⁺ T cells and IL-10⁺ Tregs are predominantly generated from infiltrating precursors at the site of infection.

FOXP3⁻IL-10⁺ CD4⁺ T cells transiently accumulated in the lung at day 7, which coincided with the beginning of response resolution (Supplementary Fig. S1A). *Il27ra*^{-/-} mice, which have been reported to have a selective deficiency in the generation of FOXP3⁻IL-10⁺ CD4⁺ T cells but not in FOXP3⁺ Tregs²⁰, were used to explore the development of FOXP3⁻IL-10⁺ CD4⁺ T cells during IAV infection. *Il27ra*^{-/-} mice lost more weight than littermate controls, exhibited a delay in post-infection weight recovery (Fig. 3A), and had a selective loss of FOXP3⁻IL-10⁺ CD4⁺ T cells in the lung (Fig. 3B–G) on day 7 of the response. There were no deficits in either IL-10⁺ or IL-10⁻ Tregs between *Il27ra*^{-/-} and control mice (Fig. 3B–D). In fact, there was a significant increase in FOXP3⁺ IL-10⁻ Tregs, potentially compensating for observed

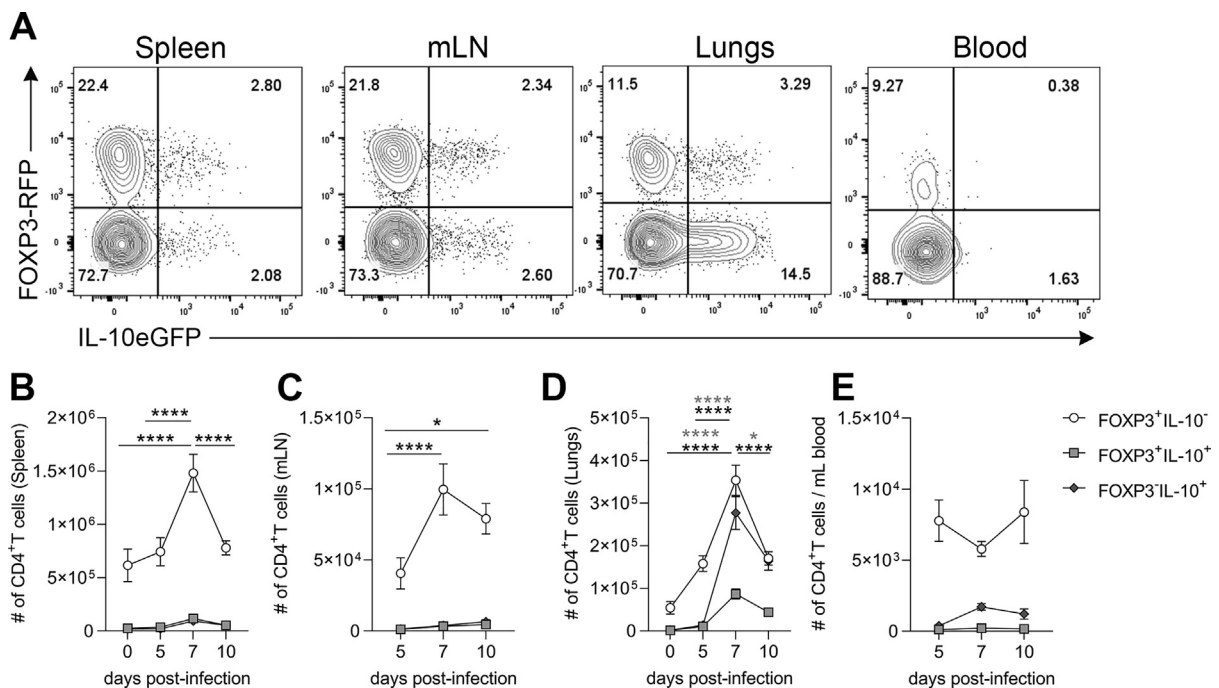


Fig. 2 FOXP3⁻IL-10⁺ CD4⁺ T cells transiently accumulate in the lung during IAV infection without significant expansion in secondary lymphoid organs. FOXP3^{RFP}IL-10^{GFP} mice were infected with X-31 IAV-intranasally and on days 0, 5, 7, and 10 post-infection spleens, mLN, lungs, and peripheral blood were harvested and activated (CD44⁺) CD4⁺ T-cell populations were quantified by flow cytometry. (A) Representative flow cytometry of CD4⁺ T-cell populations across all four organs on day 7. The number of each CD4⁺ T-cell population across the time course in the (B) spleen, (C) mLN, (D) lungs, (E) per ml of peripheral blood. Each symbol represents the mean ± standard error of mean. For spleens $n = 7-22$, mLN, $n = 10-12$, lungs $n = 7-29$, and blood $n = 7-10$, all pooled from seven independent experiments. Statistical analysis using two-way analysis of variance with Bonferroni's post-test where * $p < 0.05$, **** $p < 0.0001$. CD = clusters of differentiation; GFP = green fluorescent protein; IAV = influenza A virus; IL = interleukin; mLN = mediastinal lymph node; RFP = red fluorescent protein.

deficiency of FOXP3⁻IL-10⁺ CD4⁺ T cells. In the bronchoalveolar lavage fluid (BALF) of wild-type (WT) mice, there was an enrichment of all IL-10⁺ CD4⁺ T cells compared to the lungs, suggesting IL-10⁺ cells preferentially localize in the airways (Fig. 3E–G). Similar to the lungs, there was no reduction in Tregs between *Il27ra*^{+/+} and *Il27ra*^{-/-} mice in the BALF. However, there was a stark ablation of FOXP3⁻IL-10⁺ CD4⁺ T cells in the BALF of *Il27ra*^{-/-} mice on day 7 post-infection (Fig. 3E–G). As the *Il27ra*^{-/-} mouse is a broad knockout model, it is also known that there are potential defects in other cellular compartments such as CD8⁺ T cells, B cells, and natural killer cells^{42–44}, that may contribute to the changes in weight loss recovery post-IAV infection. However, on day 7 post-infection, we did not observe any significant differences in activated (CD44⁺) or IFN γ ⁺ CD8⁺ T cells, or T cell receptor (TCR) β ⁻ lymphocytes in terms of frequency or number in the lung (Supplementary Fig. S3). As there were no significant differences in activated CD8⁺ or CD4⁺ effector T, this could suggest that Tr1 cells are acting on a different cell type in the infected lungs such as antigen-presenting cells which have been shown in other models^{45,46}. Alternatively, as CD8⁺ T-cell numbers peak later than CD4⁺ T cells, at day 10 in the IAV-infected lungs^{47–49}, any effect of FOXP3⁻IL-10⁺ CD4⁺ T-cell-deficiency on activated CD8⁺ T cells may be observed at later time points than those analyzed in the current study. Together, these data are consistent with a role for IL-27R-dependent FOXP3⁻IL-10⁺ CD4⁺ T cells in the resolution of acute IAV infection of the lung, although further investigation utilizing transfer of antigen-specific FOXP3⁻IL-10⁺ CD4⁺ T cells will be required to implicate these cells unequivocally.

FOXP3⁻IL-10⁺ CD4⁺ T cells in IAV infection have a heterogeneous LAG-3 and CD49b surface phenotype and are localized in the parenchyma of the lungs

To explore the biology of FOXP3⁻IL-10⁺ CD4⁺ T cells in the context of acute IAV infection in more detail, we examined the expression of LAG-3 and CD49b (Supplementary Fig. S4), which have previously been described as characteristic surface markers of Tr1 cells^{23,26,27}. In this model, FOXP3⁻IL-10⁺ CD4⁺ T cells were predominately double negative (DN, LAG-3⁻CD49b⁻) during the early phase of the response (day 5 post-infection). By day 7, four populations of FOXP3⁻IL-10⁺ CD4⁺ T cells were apparent based on LAG-3 and CD49b co-expression (Fig. 4A). These include LAG-3⁺ CD49b⁺ double positive (DP) cells consistent with previously described Tr1 cells, but also substantial populations that were DN or single-positive for either LAG-3⁺ or CD49b⁺. FOXP3⁻IL-10⁺ CD4⁺ T cells that expressed at least one of these markers increased in the lung until day 7 post-infection, after which they markedly dropped in frequency (Fig. 4B). In contrast, DN

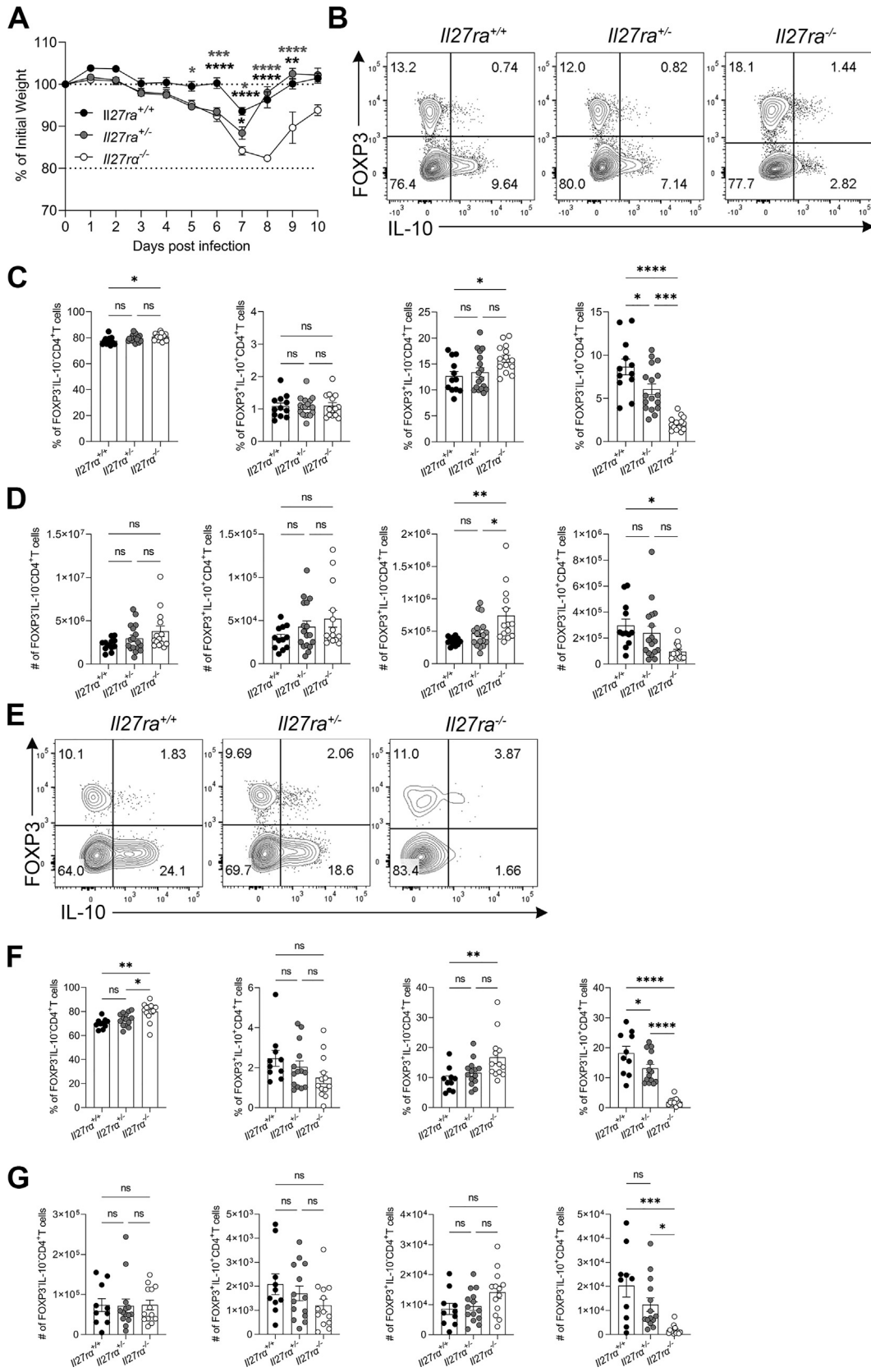
FOXP3⁻IL-10⁺ CD4⁺ T cells continued to accumulate in lung up to day 10 post-infection (Fig. 4B). FOXP3⁻IL-10⁺ CD4⁺ T-cell co-expression of IL-10 with IFN γ has been shown to align with LAG-3 and CD49b co-expression in some studies^{50,51}. Therefore, we also interrogated activated FOXP3⁻ CD4⁺ T cells in IAV, subdivided on the basis of CD49b and LAG-3 co-expression, and found that all four populations contained a population of IL-10⁺-IFN γ ⁺ cells, but that LAG-3 single-positive and DP populations were similarly enriched for co-expression of these cytokines (Supplementary Fig. S5). Together, these data define that a heterogeneous population of FOXP3⁻IL-10⁺ CD4⁺ T cells emerge during acute IAV infection. These include LAG-3⁺ CD49b⁺ DP cells consistent with previously described Tr1 cell phenotypes, although a majority of FOXP3⁻IL-10⁺ CD4⁺ T cells do not co-express LAG-3 and CD49b in this model.

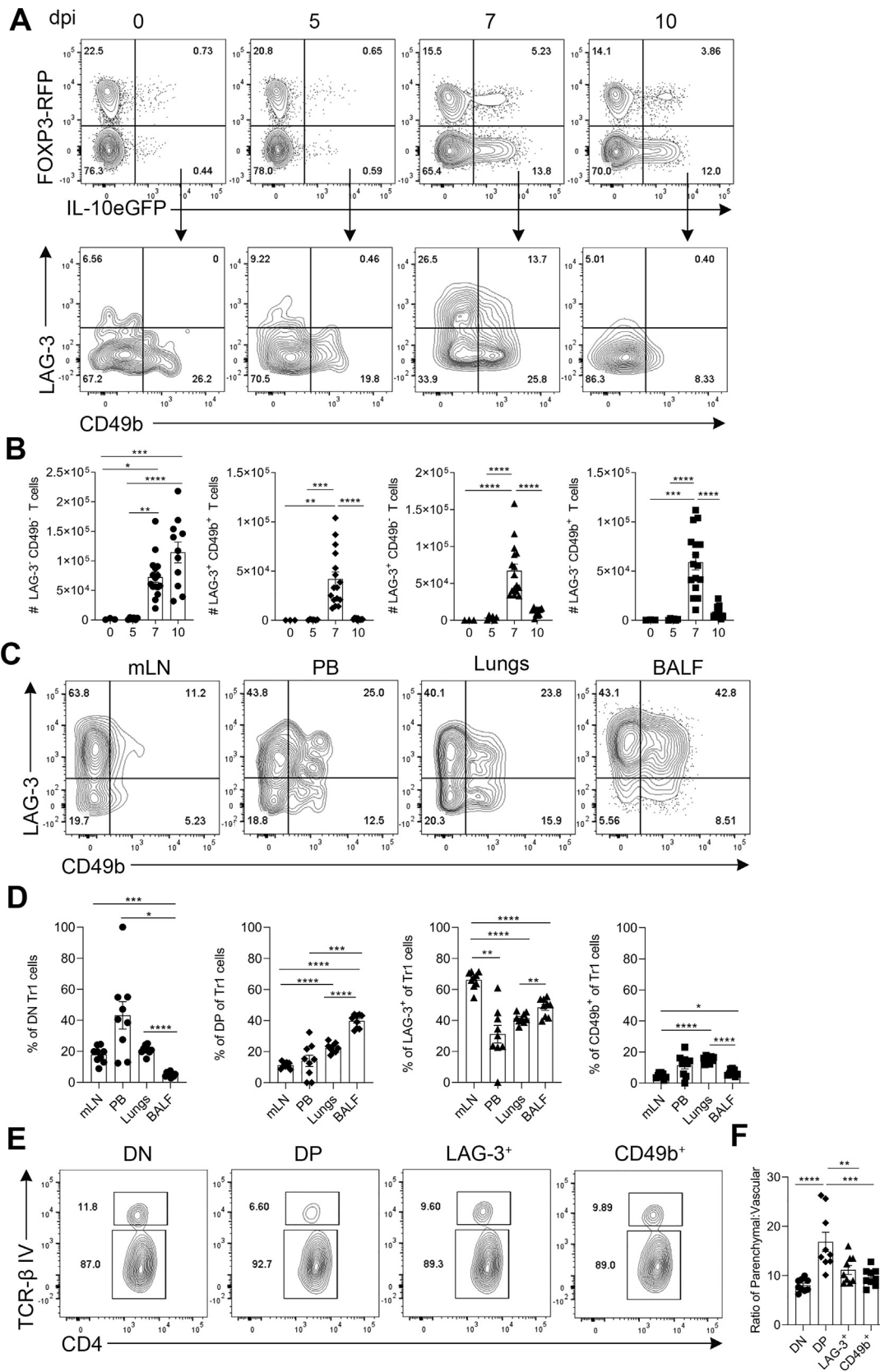
We next investigated the tissue distribution of these FOXP3⁻IL-10⁺ CD4⁺ T-cell populations based on LAG-3 and CD49b expression following acute IAV infection. The peripheral blood, mLN, lungs, and BALF were examined for the presence of FOXP3⁻IL-10⁺ CD4⁺ T cells separated on the basis of LAG-3 and CD49b on day 7 post-infection. Strikingly, LAG-3 single-positive cells were the most abundant FOXP3⁻IL-10⁺ CD4⁺ T-cell population in each of these compartments (Fig. 4C and 4D). Interestingly, DP FOXP3⁻IL-10⁺ CD4⁺ T cells were more frequent in the BALF than in other tissues examined suggesting these cells may be preferentially expanded, recruited, or maintained within the airways of infected lungs. Next, we performed intravascular labeling to determine whether these FOXP3⁻IL-10⁺ CD4⁺ T-cell populations differentially occupied the parenchyma or the vasculature of the lungs. Greater than 80% of FOXP3⁻IL-10⁺ CD4⁺ T cells were found within the parenchyma of the IAV-infected lungs on day 7 post-infection (Fig. 4E). Each of the four FOXP3⁻IL-10⁺ CD4⁺ T populations were enriched in the parenchyma compared to the vasculature of the lungs (Fig. 4E). However, the DP population was the most enriched in the parenchymal niche amongst the FOXP3⁻IL-10⁺ CD4⁺ T cells in IAV infection (Fig. 4F), suggestive of a later stage of tissue infiltration.

FOXP3⁻IL-10⁺ CD4⁺ T cells from IAV-infected lungs exhibit suppressive potential consistent with Tr1 cells

The heterogeneity observed with respect to LAG-3 and CD49b expression in the FOXP3⁻IL-10⁺ CD4⁺ T-cell compartment in acute IAV infection raised the question of whether all of these apparent Tr1-like cells are *bona fide* suppressor cells, capable of inhibiting T cell division. To address this, we performed suppression assays using labeled effector T cells. FOXP3⁻IL-10⁺ CD4⁺ T cells of each of the four identified populations were

Fig. 3 *Il27ra*^{-/-} mice exhibit a deficiency in FOXP3⁻IL-10⁺ CD4⁺ T-cells and have delayed resolution of acute IAV infection. *Il27ra*^{+/+}, *Il27ra*^{+/-}, and *Il27ra*^{-/-} mice were infected with X-31-OVA₃₂₃₋₃₃₉ IAV-intranasally and lungs were analyzed on day 7 post-infection. (A) The percentage of initial weight over the course of IAV infection. (B) Representative flow cytometry of activated CD4⁺ T-cells in the lungs at day 7 post-infection. (C) Percentage and (D) number of CD4⁺ T-cell populations in the lungs on day 7 post-infection. (E) Representative flow cytometry of activated CD4⁺ T-cells in the bronchoalveolar lavage fluid at day 7 post-infection. (F) Percentage and (G) number of CD4⁺ T-cell populations in the bronchoalveolar lavage fluid on day 7 post-infection. (A) The mean is shown \pm standard error of mean. (C–D) each symbol represents a different biological replicate, shown as mean \pm standard error of mean, $n = 12$ (*Il27ra*^{+/+}), $n = 17$ (*Il27ra*^{+/-}), $n = 14$ (*Il27ra*^{-/-}) and (F–G) $n = 10$ (*Il27ra*^{+/+}), $n = 14$ (*Il27ra*^{+/-}), $n = 13$ (*Il27ra*^{-/-}) biological replicates total from six independent experiments. Statistical analysis using (A) two-way analysis of variance, (C, D, F, & G) one-way analysis of variance both with Bonferroni's correction * $p \leq 0.05$, ** $p \leq 0.01$, *** $p \leq 0.001$, **** $p \leq 0.0001$. CD = clusters of differentiation; IAV = influenza A virus; IL = interleukin.





sorted from the lungs of IAV-infected FOXP3^{RFP}IL-10^{GFP} mice on day 7 post-infection for these assays (Supplementary Fig. S6). All four FOXP3⁻IL-10⁺ CD4⁺ T-cell populations were capable of significant titratable inhibition of effector T cell division (Fig. 5A–C), with the DP and LAG-3⁺ populations most suppressive on a per cell basis (significantly suppressive out to a 1:8 FOXP3⁻IL-10⁺ CD4⁺ T:effector T cell ratio) (Fig. 5B). All four populations of FOXP3⁻IL-10⁺ CD4⁺ T cells were similarly as suppressive in these assays as FOXP3⁺ Tregs (Fig. 5) and significantly more suppressive than co-cultured effector T cells used as negative controls (Fig. 5). These results indicate that all four populations of FOXP3⁻IL-10⁺ CD4⁺ T cells in IAV exhibit suppressive potential, consistent with the current definition of Tr1 cells. Notably, the DP and LAG-3⁺ Tr1 cells exhibited the most potent regulatory activity, but this was not a substantial difference in suppressive capacity in these assays. Mechanistically, Tr1 cells have been reported to exert suppression predominately via IL-10 production^{11,27,52}. Thus, each of the four Tr1 cell populations was tested for their dependence on IL-10 to elicit suppression by conducting assays with a neutralizing α -IL-10R α antibody (Fig. 5D and 5E). DP and CD49b⁺ Tr1 cells exhibited some dependence on IL-10 to elicit suppression, while DN and LAG-3⁺ Tr1 cells suppressed effector T cell division independently of IL-10 (Fig. 5D and 5E). Although IL-10 was important for suppression exerted by DP and CD49b⁺ populations of Tr1 cells, this indicated that other mechanisms were employed by LAG-3⁺ and DN Tr1 cells to inhibit effector T cell division.

Transcriptomic analysis of lung-derived Tr1 populations

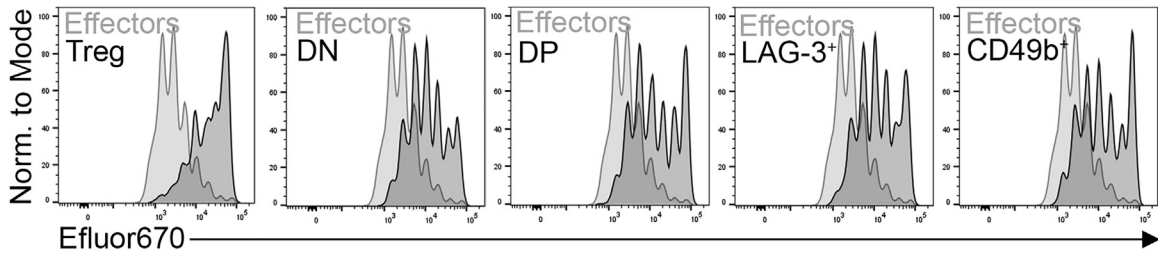
Given the differences observed in kinetics, localization, and dependence on IL-10 for suppressive capacity between the four Tr1 cell populations identified in IAV infection, further differences were probed at the transcriptional level. RNA sequencing was conducted on each of the four populations sorted from lungs of IAV-infected FOXP3^{RFP}IL-10^{GFP} mice on day 7 post-infection (Supplementary Fig. S7). Using a false discovery rate (FDR) < 0.05 and estimated log-fold-change (logFC) greater/less than 1(+/-1), 243 differentially expressed (DE) genes were identified in total (where each unique gene was determined to be DE in at least one comparison). An UpSet plot was generated from a list of the DE genes across all six comparisons. This analysis revealed that the LAG-3⁺ and CD49b⁺ populations exhibited 169 DE genes, the greatest number in any one comparison and consequently appeared the most distinct among all the popula-

tions (Fig. 6A). Unique gene set signatures were determined for the DN, LAG-3⁺, and CD49b⁺ Tr1 cell populations but not for the DP Tr1 cells (Fig. 6A, Supplementary Fig. S8A). This is likely due to the DP sharing features of both the LAG-3⁺ and CD49b⁺ Tr1 cells meaning there are no significant uniquely expressed genes by this population. Next, it was established how closely each of the four Tr1 cell populations from acutely infected mice resembled previously reported Tr1 cells and other CD4⁺ T-cell subsets. To address this, a list of Tr1 cell signature genes was compiled from previous studies^{19,21,23,27,30}. We compared the expression of Tr1 signature genes as well as genes associated with Th1, Th2, Th17, Tfh, and Tregs between the four Tr1 cell populations from IAV-infected lungs. Apart from the genes encoding the surface markers used for their differential sorting, it was apparent that all four populations of Tr1 cells strongly conform to a core Tr1 cell gene expression signature (i.e. abundant *Il10*, *Maf*, *Gzmb*, *Icos*, *Tigit*, *Ctla4*, and *Pdcd1*) (Fig. 6B). An exception amongst these Tr1 cell-associated genes was *Eomes*, which encodes a transcription factor that has been shown to control Tr1 cell development during chronic alloantigen exposure in graft-versus-host disease³¹. In acute IAV, *Eomes* were not highly expressed in Tr1 cells but were present at low levels only in the two CD49b⁻ Tr1 cell populations. This was confirmed by staining intracellular EOMES protein in these cells (Supplementary Fig. S9). In addition, acute IAV infection-induced Tr1 cells generally did not express high levels of genes associated with Th2 (except *Gata3*), Th17, Tfh, or Tregs (except *Il2ra* and *Il2rb*) but did abundantly express Th1-associated genes including *Tbx21*, *Cxcr3*, *Cxcr6*, and *Ifng*. Together, these data indicate that the Tr1 cell populations that arise during acute IAV infection strongly resemble previously described Tr1 cells and that the LAG-3⁺ and CD49b⁺ populations were the most transcriptionally distinct amongst these populations.

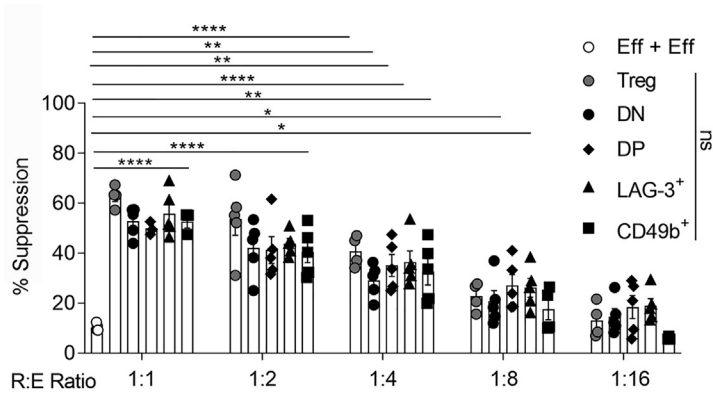
Next, to further explore differences between Tr1 cell populations, pathway analysis was conducted to identify the gene ontologies (GO) significantly enriched in each comparison. First, DN and LAG-3⁺ Tr1 cells were compared, and this revealed 58 GO terms significantly enriched including 'inflammatory response' highlighting genes such as *Havcr2*, *Cst7*, and *Lag3* expressed by the LAG-3⁺ Tr1 cells (Supplementary Fig. S9C). Between the LAG-3⁺ and DP Tr1 cells, five significantly enriched GO terms were identified including 'transmembrane receptor activity' (e.g. *Cxcr5*, *Itga2*, *Klrl1*, and *Gpr15*) (Fig. 6C). DP Tr1 cells expressed more *Itga2*, *Klrl1*, and *Gpr15*, whereas LAG-3⁺ Tr1 cells

Fig. 4 IAV-induced FOXP3⁻IL-10⁺ CD4⁺ T-cells exhibit heterogeneous expression of LAG-3 and CD49b and are localized in the lung parenchyma. FOXP3^{RFP}IL-10^{GFP} mice were infected with X-31 IAV-intranasally. (A) On days 0, 5, 7, and 10 post-infection lungs were harvested. Concatenated representative flow cytometry depicting expression of FOXP3 and IL-10 by activated CD4⁺ T-cells and LAG-3 and CD49b by FOXP3⁻IL-10⁺ CD4⁺ T-cells. (B) The number of LAG-3⁺ CD49b⁻, LAG-3⁺ CD49b⁺, LAG-3⁻ CD49b⁻, and LAG-3⁻ CD49b⁺ FOXP3⁻IL-10⁺ CD4⁺ T-cells post-IAV infection. (C) Concatenated representative flow cytometry from the indicated organs at day 7 post-infection, displaying LAG-3 and CD49b expression by FOXP3⁻IL-10⁺ CD4⁺ T-cells. (D) Frequency of DN, DP, LAG-3⁺, and CD49b⁺ FOXP3⁻IL-10⁺ CD4⁺ T-cells in the mLN, PB, lungs, and BALF. (E) Concatenated flow cytometry depicting TCR- β I.V labeling (top TCR- β ⁺ gate in E) of FOXP3⁻IL-10⁺ CD4⁺ T-cells from the lungs on day 7 post-infection. (F) The ratio of FOXP3⁻IL-10⁺ CD4⁺ T-cells in the parenchyma versus the vasculature. Each symbol represents a different biological replicate, bars show the mean, and error bars depict \pm standard error of mean, (A–B) $n = 3–15$ biological replicates total per time point from three independent experiments, (C–F) $n = 9$ biological replicates total from two independent experiments. Statistical analysis using (B, D, F) one-way analysis of variance with Bonferroni's post-test * $p \leq 0.05$, ** $p \leq 0.01$, *** $p \leq 0.001$, **** $p \leq 0.0001$. BALF = bronchoalveolar lavage fluid; CD = clusters of differentiation; DN = double negative; DP = double positive; GFP = green fluorescent protein; IAV = influenza A virus; IL = interleukin; I.V = intravenous; LAG-3 = lymphocyte activation gene-3; mLN = mediastinal lymph node; PB = peripheral blood; RFP = red fluorescent protein; TCR = T cell receptor.

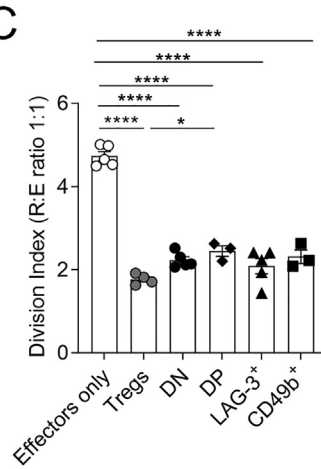
A



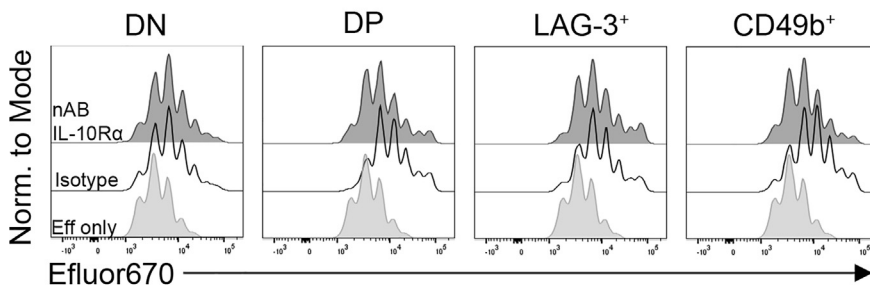
B



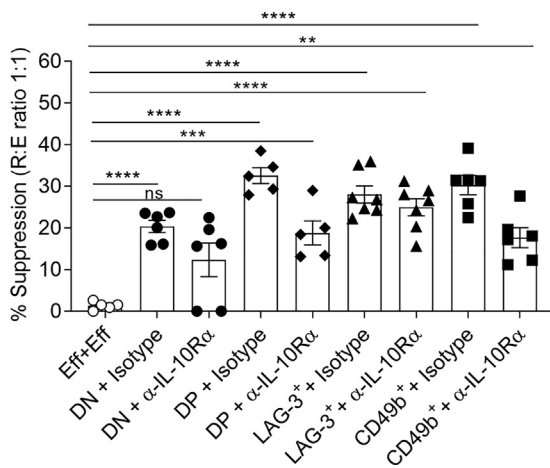
C



D



E



expressed more *Cxcr5*. This suggested the DP Tr1 cells expressed more genes associated with T-cell activation and adhesion than LAG-3⁺ Tr1 cells and therefore potentially constitute a more differentiated population. Between CD49b⁺ and DP Tr1 cells only 2 GO terms were considered significantly enriched. These included 'extracellular space' (e.g. *Fam20a*, *Igfbp7*, *Lgals7*, *Areg*, *S100a8*, *Cst7*, *Csf1*, *S100a9*, and *Pla1a*) (Fig. 6D). The 'extracellular space' GO term encompasses genes encoding surface and secreted molecules that were DE by the DP Tr1 cells and could thus be attributed a more activated and functional cell phenotype. The comparison between LAG-3⁺ and CD49b⁺ Tr1 cells identified 47 significantly enriched GO terms including 'cell-cell adhesion' (e.g. *Lgals7*, *Perp*, *Tespa1*, *Lag3*, *Itgb3*, *Itga2*, and *Il10*) (Fig. 6E). This analysis indicated that CD49b⁺ Tr1 cells expressed increased levels of integrins and exhibited a more terminally differentiated gene signature than LAG-3⁺ Tr1 cells. Collectively, the pathway analysis identified differences in GO terms associated with activation and adhesion suggesting that the major differences in these Tr1 populations are related to their activation and functional state with DP cells potentially representing the most activated population.

Upon examining expression of specific genes between the four Tr1 populations in more detail it was apparent that LAG-3⁺ Tr1 cells exhibited a more activated and regulatory profile than DN Tr1 cells (e.g. increased expression of *Havcr2*, *Lag3*, and *Areg*) (Fig. 6F). Indeed, compared to each of the other populations DN Tr1 cells appeared more Tfh-like, suggestive of a less differentiated or stem-like activation state (Fig. 6F, Supplementary Fig. S9). Comparison between LAG-3⁺ and DP Tr1 cells revealed DE genes upregulated in LAG-3⁺ Tr1 cells that were suggestive of a less differentiated state (e.g. *Sell* and *Cxcr5*) (Fig. 6G). In contrast, genes increased in DP Tr1 cells were consistent with a more activated and functional phenotype than the LAG-3⁺ Tr1 cells (e.g. DE genes included *Klrk1*, *Klrg1*, *Gzmm*, and *Itga2*) (Fig. 6G). Consistent with the observations from the GO term analysis, compared to both LAG-3⁺ and DP cells, CD49b⁺ Tr1 cells exhibited more features of active TCR signaling (e.g. *Tespa1* and *Trat1*) in combination with increased expression of receptors associated with induction of cell death (e.g. *P2rx7*

and *Tnfrsf25*) (Fig. 6H and 6I), which implied a more apoptotic phenotype of CD49b⁺ Tr1 cells. Thus, there are differences apparent in the expression of genes associated with T-cell activation and fitness between the various Tr1 cell populations from lungs of acutely infected mice. Together this suggests the four populations identified in our model based on expression of LAG-3 and CD49b correspond to a dynamic developmental trajectory for Tr1 cells, where LAG-3⁺ and DP populations appear to represent a classical Tr1 signature, with LAG-3⁺ Tr1 cells perhaps less mature than DP cells. DN cells exhibit a more stem-like signature and express Tfh-like genes, whereas the CD49b population enriches for a more apoptotic signature perhaps correlating with terminal differentiation. Therefore, each population appears to correspond with a state of activation and function for FOXP3⁻IL-10⁺ CD4⁺ T cells.

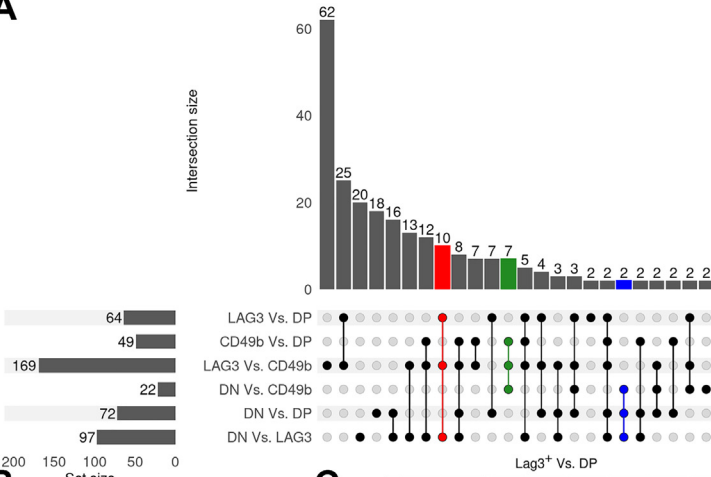
Tr1 cell populations exhibit differences in activation and fitness

As genes associated with activation and death were highly DE between the four populations of Tr1 cells, several of these were probed further. T cell immunoglobulin and mucin domain-containing protein 3 (TIM-3) and programmed cell death protein 1 (PD-1) (activation markers induced upon TCR signaling and activation)^{53–55} were first selected for further investigation. Tr1 cells express a range of co-inhibitory receptors²³, and expression of receptors including PD-1 and TIM-3 has been shown to mark suppressor cell populations in a number of different contexts^{11,56,57}. Expression of such receptors is also an indication of activation and antigen experience⁵³, thereby allowing their co-expression to provide a readout of the activation level of Tr1 cells. Both DP and LAG-3⁺ Tr1 cells expressed significantly greater surface PD-1 compared to DN and CD49b⁺ Tr1 cells (Fig. 7A and 7B). Furthermore, the DP Tr1 cells expressed the highest level of surface TIM-3 and exhibited the greatest proportion of PD-1⁺ TIM-3⁺ double positive cells (Fig. 7A and 7D), further supporting the notion that DP Tr1 cells are the most activated of the four populations.

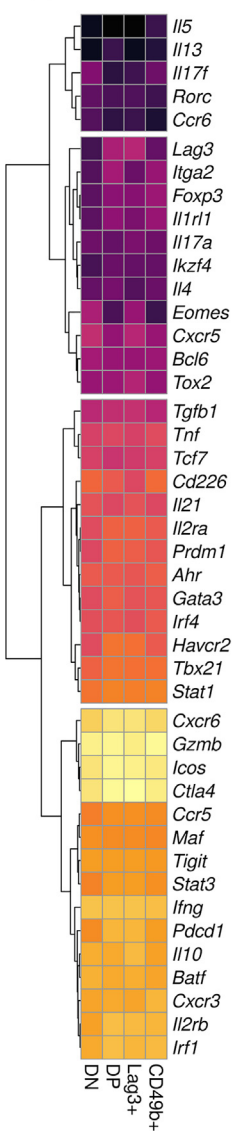
P2RX7 is a surface purinergic receptor that senses extracellular adenosine triphosphate and can induce apoptosis⁵⁸. It has

Fig. 5 FOXP3⁻IL-10⁺ CD4⁺ T-cells induced by IAV infection are capable of suppressing effector T-cell division. FOXP3^{RFP}IL-10^{GFP} mice were infected with X-31 IAV-intranasally and FOXP3⁻IL-10⁺ CD4⁺ T-cell populations were fluorescence-activated cell sorting (FACS)-sorted from lungs on day 7 post-infection for suppression assays. (A) Representative flow cytometry showing the proliferation of Efluor670-labeled CD3⁺CD25⁻ responder T cells with stimulation alone (light gray histograms, Effectors) or in the presence of either Treg cells (CD4⁺FOXP3⁺CD25⁺) sorted from naïve FOXP3^{RFP}IL-10^{GFP} mouse secondary lymphoid organs (as a positive control for suppression), or each of the FOXP3⁻IL-10⁺ CD4⁺ T-cells (overlaid dark gray histogram) at a 1:1 ratio (2×10^4 Tr1 cells: 2×10^4 effector T cells). (B) The percentage suppression of effector T cell division at each ratio of Treg cells or FOXP3⁻IL-10⁺ CD4⁺ T cells: effector T cells (1:1–1:16) compared to effector T cells cultured with effector T cells (Eff + Eff). (C) Division index of effector T cells cultured with APCs and α -CD3 alone or with either Treg cells or FOXP3⁻IL-10⁺ CD4⁺ T-cells at a 1:1 ratio (where division index = the mean number of divisions within a population). (D) Representative flow cytometry depicting division of labeled effector T cells from suppression assays. Stimulation alone condition (light gray histograms), co-cultured with each of the FOXP3⁻IL-10⁺ CD4⁺ T-cell populations (1:1 ratio) in the presence of an isotype control (black histograms), in the presence of IL-10Ra nAb (dark gray histograms). Data are shown as mean \pm standard error of mean, (A–C) $n = 3–5$ biological replicates, (D & E) $n = 4–7$ replicates from three independent experiments. Statistical analysis using (B), (C) one-way analysis of variance with Bonferroni's post-test between the Eff + Eff and each Treg and FOXP3⁻IL-10⁺ CD4⁺ T-cell population. Two-way analysis of variance with Bonferroni's post-test was also used to compare the percentage suppression observed for Treg cells and there were no statistically significant differences when compared with the suppression observed for the FOXP3⁻IL-10⁺ CD4⁺ T-cell populations. (E) One-way analysis of variance with Bonferroni's post-test between the Eff + Eff and each FOXP3⁻IL-10⁺ CD4⁺ T-cell population * $p < 0.05$, ** $p < 0.01$, *** $p < 0.001$, **** $p < 0.0001$. APCs = antigen presenting cells; CD = clusters of differentiation; DN = double negative; DP = double positive; GFP = green fluorescent protein; IAV = influenza A virus; IL = interleukin; nAb = neutralising antibody; RFP = red fluorescent protein; TCR = T cell receptor; Treg = regulatory T cell, Tr1 = type 1 regulatory.

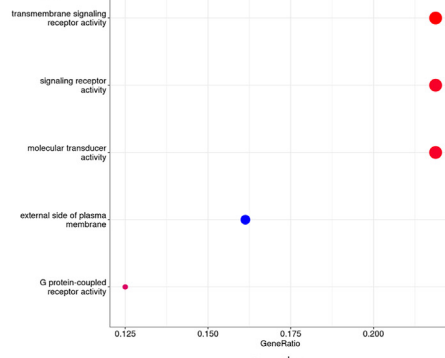
A



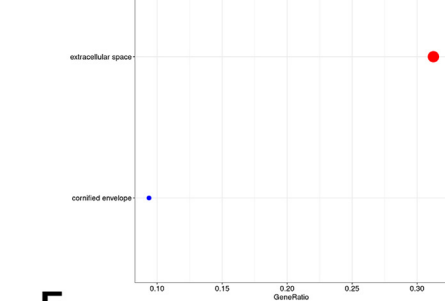
B



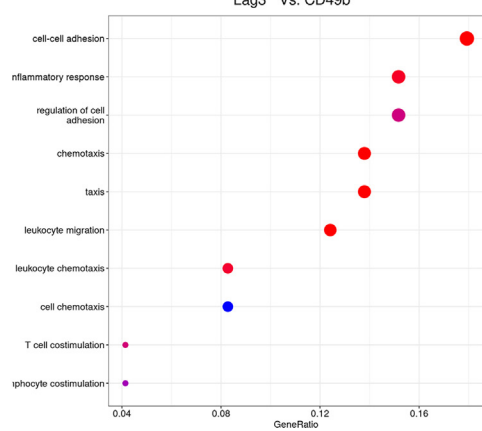
C



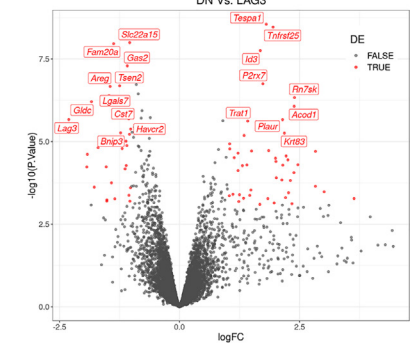
D



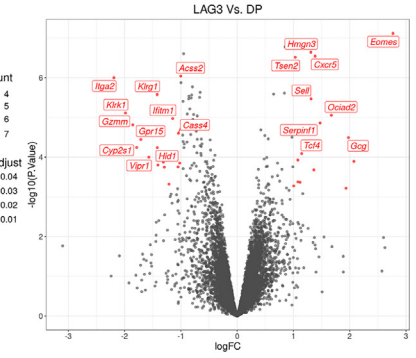
E



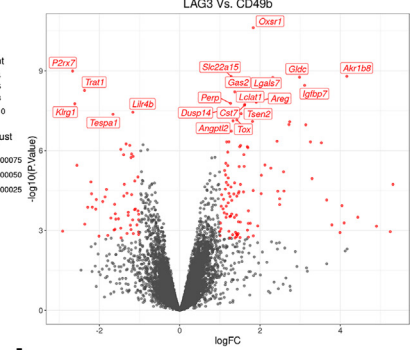
F



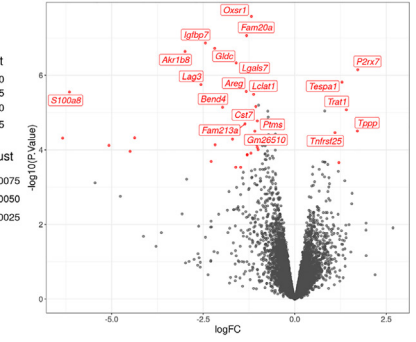
G



H



I



also been shown to regulate metabolic fitness in CD8⁺ T cells⁵⁹ but has not previously been implicated in Tr1 cell function. *P2rx7* was found to be most highly expressed by CD49b⁺ Tr1 populations (Supplementary Fig. S9). In keeping with this, flow cytometric analysis revealed a significantly higher percentage of CD49b⁺ Tr1 cells were P2RX7⁺ compared to DP and LAG-3⁺ Tr1 cells (Fig. 7E and 7F). Whether there were differences in fitness, proliferative capacity, and survival between the Tr1 cell populations was assessed by Ki67, Annexin V, and 7AAD staining. No differences were observed in cell cycling as reported by intranuclear Ki67 staining (Fig. 7G and 7H). However, when assessing fitness and death, DP and CD49b⁺ Tr1 cells contained a greater frequency of pre-apoptotic Annexin V⁺ cells compared to the other populations (Fig. 7I–L). In addition, the CD49b⁺ population contained the greatest proportion of 7AAD and Annexin V dual-positive cells that had undergone apoptosis (Fig. 7I–L). These data are consistent with CD49b⁺ Tr1 cells undergoing a higher rate of apoptosis than the other Tr1 cell subsets and further suggest that CD49b⁺ Tr1 cells represent a more terminally differentiated Tr1 cell population. Altogether, the transcriptional and functional data suggested a possible step-wise increase in T-cell activation from DN to LAG-3⁺ to DP, with CD49b⁺ Tr1 cells representing an activated population that had increased susceptibility to apoptosis.

Plasticity of lung-derived Tr1 cells generated in response to IAV infection

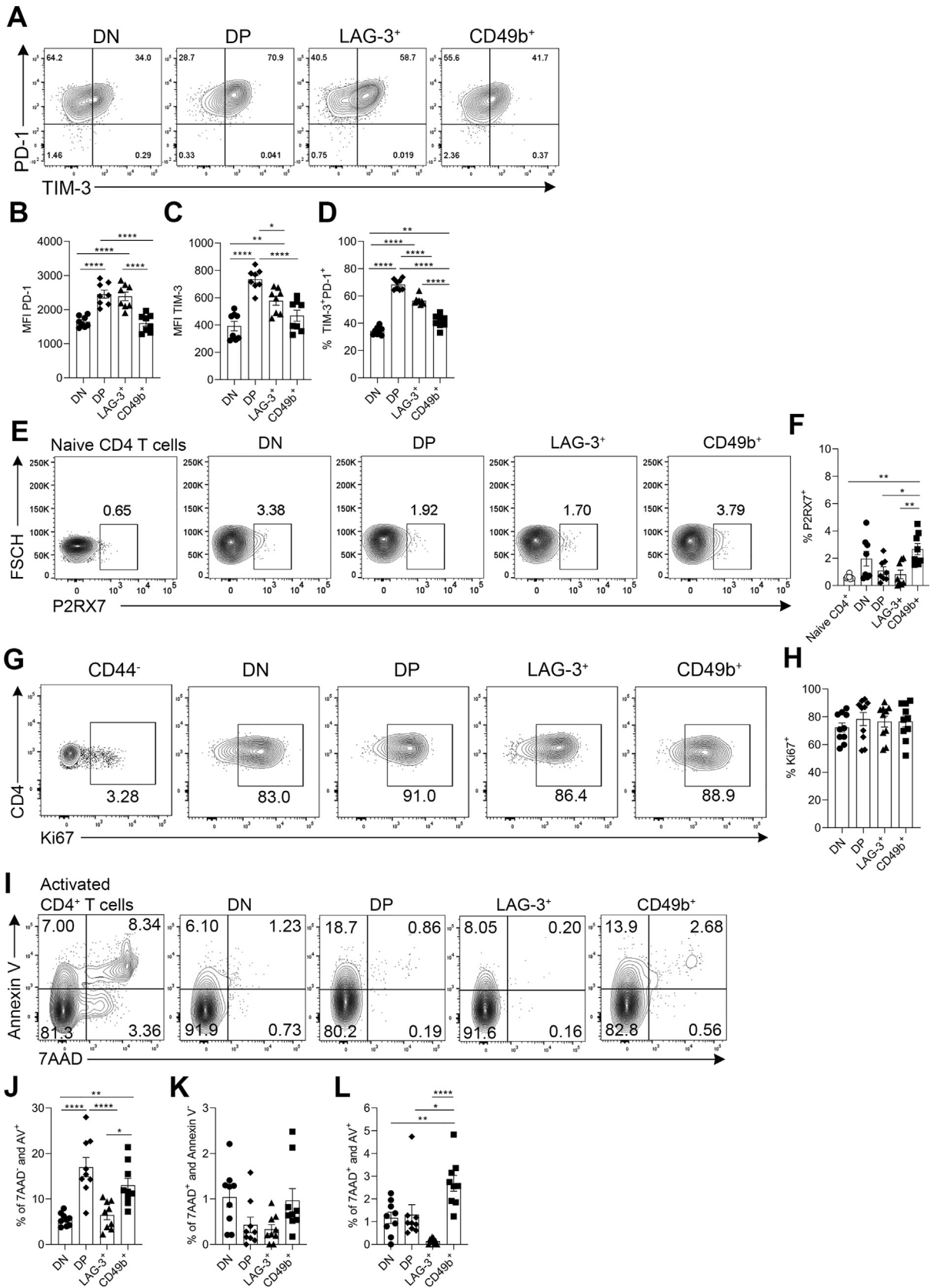
To test whether an exclusively linear step-wise progression between the four Tr1 cell populations observed in IAV infection exists, an adoptive transfer strategy was utilized. Each of the four Tr1 cell populations was FACS-sorted from lungs on day 7 post-infection (Supplementary Fig. S10) and transferred into infection-matched WT hosts. Due to the technical challenges of working with small numbers of lung-derived Tr1 cells, despite pooling from multiple experiments, insufficient DN, DP, and CD49b⁺ Tr1 cells were recovered following transfer for robust analysis of their fate and plasticity. However, as the dominant population of Tr1 cells, the LAG-3⁺ Tr1 cells could be tracked reliably and were sufficient to test the hypothesis that Tr1 cells undergo a unidirectional linear progression through the observed populations during acute IAV infection. On day 9 post-infection, tissues were collected for analysis of transferred cells (Fig. 8A). Transferred cells were detected in the lungs (Fig. 8B, 8E–G) and spleen (Fig. 8H–J) of recipient mice. LAG-3⁺

Tr1 cells predominately maintained expression of IL-10 post-transfer and did not begin to express FOXP3 regardless of tissue of recovery (Fig. 8D, 8E, and 8H), indicating a degree of stability of the Tr1 cell phenotype, at least across this period of time. Regarding plasticity of LAG-3 and CD49b co-expression, LAG-3⁺ Tr1 cells either maintained their LAG-3⁺ profile or adopted either a DP or DN profile following adoptive transfer. Very few LAG-3⁺ Tr1 cells converted to a CD49b⁺ single-positive profile over the period of time analyzed (Fig. 8F and 8G). Transferred LAG-3⁺ Tr1 cells recovered from the lungs and spleens exhibited a different distribution of surface expression of LAG-3 and CD49b, with less conversion to a DN phenotype apparent in the spleen than in the lung. Together, these experiments determined that LAG-3⁺ Tr1 cells exhibit stable IL-10 production but have the potential to rapidly adopt different expression profiles of LAG-3 and CD49b co-expression. Despite being limited to evaluation of transfer of the LAG-3⁺ Tr1 cells, these data establish that there is significant plasticity in Tr1 cell populations during IAV infection and that there is not a uniform linear step-wise progression evident through Tr1 cell fates.

DISCUSSION

Tr1 cells have been shown to play an important regulatory role by suppressing effector responses that limit chronic inflammation^{60–62}. In this study, we have shown these IL-27R-dependent FOXP3⁺IL-10⁺ CD4⁺ T cells are the dominant T-cell source of IL-10 in the lung of IAV-infected mice, greatly outnumbering IL-10⁺ Tregs, and in their absence there is delayed recovery from infection-induced weight loss, consistent with a role for Tr1 cells during the resolution of acute inflammation and similar to that described for these cells in chronic inflammation²². However, as the model used for Tr1 cell deficiency in this study removes all IL-27R-dependent elements of the immune response, to specifically prove direct involvement of Tr1 cells in the resolution of acute IAV infection, adoptive transfer of Tr1 cells into IAV-infected *Il27ra*^{-/-} mice will be required in future. Given previous studies^{11,57,63,64}, it is likely that this will require the use of antigen-specific Tr1 cells. In this context, it will be important to elucidate any Tr1 cell-dependent effect on the histopathological status of IAV-infected lungs. Previous studies have shown that transferred memory Tregs significantly attenuate lung pathology in IAV-infected mice^{7,65} so it will be of interest in future to determine whether Tr1-mediated regulation of inflammation in the IAV-infected lung has a similar impact. Intriguingly, we also

Fig. 6 Four populations of IAV-induced Tr1 cells conform to a general Tr1 cell gene expression signature but exhibit transcriptional divergence consistent with different activation states. FOXP3^{RFP}IL-10^{GFP} mice were infected with X-31 IAV-intranasally and on day 7 post-infection DN, DP, CD49b⁺ and LAG-3⁺ subsets of Tr1 cells were FACS-sorted and analyzed by RNA sequencing. (A) UpSet plot for all DE genes. (B) Heatmap depicting average messenger RNA expression of a range of genes known to be associated with CD4⁺ T-cell lineages across the four Tr1 populations (generated using pheatmap in RStudio). The heatmap scale refers to the average logCPM on a continuous scale for each gene listed. (C–E) Pathway analysis was conducted using clusterProfiler in R studio and dot plots are shown for the comparisons between (C) Lag3⁺ versus DP, (D) Cd49b⁺ versus DP, and (E) Lag3⁺ versus CD49b⁺. Dot size is proportional to the number of genes in a given EntrezID gene set and a Bonferroni-adjusted $p < 0.05$ was used as a cut-off for significantly enriched pathways. (F–I) Volcano plots were generated using ggplot2 in R studio with comparisons between (F) DN versus LAG-3⁺, (G) LAG-3⁺ versus DP (H) Lag3⁺ versus CD49b⁺, and (I) CD49b⁺ versus DP. The top 20 differentially expressed genes are labeled in each comparison. Colored dots indicate significantly differentially expressed genes based on a FDR < 0.05 and an estimated logFC greater than/less than ±1. N = 4 biological replicates for each population from two independent experiments were analyzed for RNA sequencing. CD = clusters of differentiation; CPM = counts per million; DE = differentially expressed; DN = double negative; DP = double positive; FC = fold-change; FDR = false discovery rate; GFP = green fluorescent protein; IAV = influenza A virus; IL = interleukin; LAG-3 = lymphocyte activation gene-3; RFP = red fluorescent protein; TCR = T cell receptor; Tr1 = type I regulatory cell.



reveal that Tr1 cells generated in response to IAV infection exhibit heterogeneous expression of the Tr1 cell characteristic markers, LAG-3 and CD49b. Four Tr1 cell populations were identified which exhibited differences in their kinetics, phenotype, and potential function and corresponded to different states of activation for Tr1 cells. Using this model of Tr1 cell generation in acute infection we have revealed multiple novel insights into Tr1 cell biology, including new information on their development, heterogeneity, mechanisms of suppression, and phenotypic stability.

In this study, we identified four populations of FOXP3⁻IL-10⁺ CD4⁺ T cells based on expression of LAG-3 and CD49b. This study builds on previous work identifying IL-10-producing CD4⁺ T cells in IAV infection^{26,32,33}, by determining that these cells are consistent with Tr1 cells by current defining characteristics and further investigating their biology. While we found that >75% of FOXP3⁻IL-10⁺ T cells found in lungs of IAV-infected do not co-express LAG-3 and CD49b, these cells meet all other defining criteria of Tr1 cells (i.e. are capable of suppressing bystander T cell proliferation and do not produce IL-4 or IL-17A)¹⁸. While we do not query that LAG-3 and CD49b are useful surface markers for enrichment of Tr1 cells from humans, it is clear in this model of acute infection in mice that cells meeting all other defining criteria of Tr1 cells are not exclusively DP. Our transcriptomic analysis indicated that DP Tr1 cells expressed more genes associated with T-cell functionality and also had the highest level of TIM-3 expression, which may indicate that DP Tr1 cells represent a more tissue-infiltrated and functionally active stage of Tr1 cell biology than the other populations. Indeed, we found that a substantial fraction of LAG-3⁺ Tr1 cells converted to DP following transfer and also revealed that DP Tr1 cells were found deeper within the infected tissue (more parenchymal and localized in airways) than other populations of Tr1 cells. Overall, the current study has established significant heterogeneity within the Tr1 cell compartment during acute infection. Although DP Tr1 cells were not the only population identified, they did appear to express the most genes associated with regulatory function and hence may represent the most functional Tr1 cells.

One important feature of the different populations of Tr1 cells that emerged during acute IAV infection was differential dependence on IL-10 for suppression. Specifically, DP and CD49b⁺ cells utilized IL-10 but the other Tr1 cell populations were suppressed independently of IL-10. Moreover, neutralizing IL-10 only partially inhibited suppression by DP and CD49b⁺ cells. Together, these observations indicate that other molecular mechanisms are used by those cells to exert suppression. While the mechanisms by which Tr1 cells exert suppression *in vivo*

remain incompletely understood and vary from study to study, the most commonly reported mechanisms reported to be used by Tr1 cells to suppress effector T-cell division are either IL-10 or via co-inhibitory receptors. For example, Tr1 cell-mediated suppression by Tr1 cells isolated from a model of colitis is dependent on IL-10^{51,66}. However, post α -CD3 treatment, small intestinal Tr1 cells were enriched for expression of many co-inhibitory receptors and potently suppressed effector T-cell proliferation *in vitro*, whereas splenic Tr1 cells from the same mice expressed fewer co-inhibitory receptors and were not as suppressive²³. In addition, Tr1 cells in models of antigen tolerization and allergy were shown to inhibit T-cell proliferation via cell-contact mediated mechanisms dependent on binding to PD-1 and CTLA-4 on target cells^{24,25,56}. Studies of Tallo10 cells, a polarized human Tr1 cell clinical product, have revealed that Tr1 cells in this context suppress T-cell proliferation via cell-contact mechanisms through binding CTLA-4 and PD-1, as well as via soluble IL-10⁵⁷. Given the results from the current study, it will be of interest to determine any cell-contact-dependent mechanisms of suppression mediated by Tr1 cell subpopulations isolated from IAV-infected lungs. Notably, DN Tr1 cells are suppressive independently of IL-10 and do not express LAG-3, which rules out a contribution of LAG-3 to their suppressive capacity. Other mechanisms potentially contributing to the suppressive function of Tr1 cells include PD-L1 ligation of effector T cell PD-1 or secreted transforming growth factor- β . Thus, further investigation is required to elucidate the mechanisms used by IAV-derived Tr1 cells to suppress T-cell division.

The circumstances under which Tr1 cells emerge contribute to immune responses, and their subsequent fate remains somewhat enigmatic. Currently, it is not definitively known whether these cells emerge *in vivo* directly from naïve precursors or adopt an IL-10-secreting phenotype after transitioning through another effector program, or can come from either pathway^{19,21,22,26}. Analysis of the appearance of Tr1 cells in the present study indicates that, unlike Tregs, Tr1 cells do not substantially increase in frequency in draining lymph node or spleen following infection but accumulate abruptly in lungs on day 7. This indicates that it is likely that a substantial fraction of Tr1 cells derives from effector T cells that adopt IL-10 expression *in situ*. However, this will require future analysis of appropriate fate-reporter mice, such as has been shown for Th17 cells that transition to Tr1 in the context of autoimmunity²². The kinetics of the appearance of Tr1 cells in the present study are quite consistent with previous studies in lymphocytic choriomeningitis (LCMV), *N.Brasiliensis* infection, and following lethal influenza infection^{26,27}, where these cells were also noted to appear between day 5 and day 7. However, the kinetics of the

Fig. 7 Activation, proliferation, and death of Tr1 cell populations. FOXP3^{RFP}IL-10^{GFP} mice were infected with X-31 IAV-intranasally and lungs were harvested on day 7 post-infection. (A) Representative flow cytometry of TIM-3 and PD-1 co-expression by Tr1 cells. MFI of (B) PD-1 and (C) TIM-3. (D) The percentage of PD-1 TIM-3 DP cells. (E) Representative flow cytometry of P2RX7 expression by each of the four Tr1 cell populations compared to naïve CD4⁺ T-cells. (F) Frequency of P2RX7⁺ cells. (G) Representative flow cytometry depicting expression of intranuclear Ki67 by Tr1 cells. (H) Frequency of Ki67⁺ of each of the Tr1 populations. (I) Representative flow cytometry of annexin V and 7AAD co-staining. Frequency of (J) 7AAD⁺AV⁺, (K) 7AAD⁺AV⁻, and (L) 7AAD⁺AV⁺ Tr1 cells. Each symbol is a different biological replicate, data shown as mean \pm standard error of mean, (B–D) $n = 8$, (F) $n = 8$, and (J–L) $n = 9$ biological replicates total from two independent experiments. Statistical analysis using one-way analysis of variance with Bonferroni's post-test * $p < 0.05$, ** $p < 0.01$, *** $p < 0.001$, **** $p < 0.0001$. AV = annexin V; CD = clusters of differentiation; DN = double negative; DP = double positive; GFP = green fluorescent protein; IAV = influenza A virus; IL = interleukin; PD-1 = programmed cell death protein 1; P2RX7 = purinergic receptor P2X7; RFP = red fluorescent protein; TIM-3 = T cell immunoglobulin and mucin domain-containing protein 3; Tr1 = type I regulatory cell; 7AAD = 7-aminoactinomycin D.

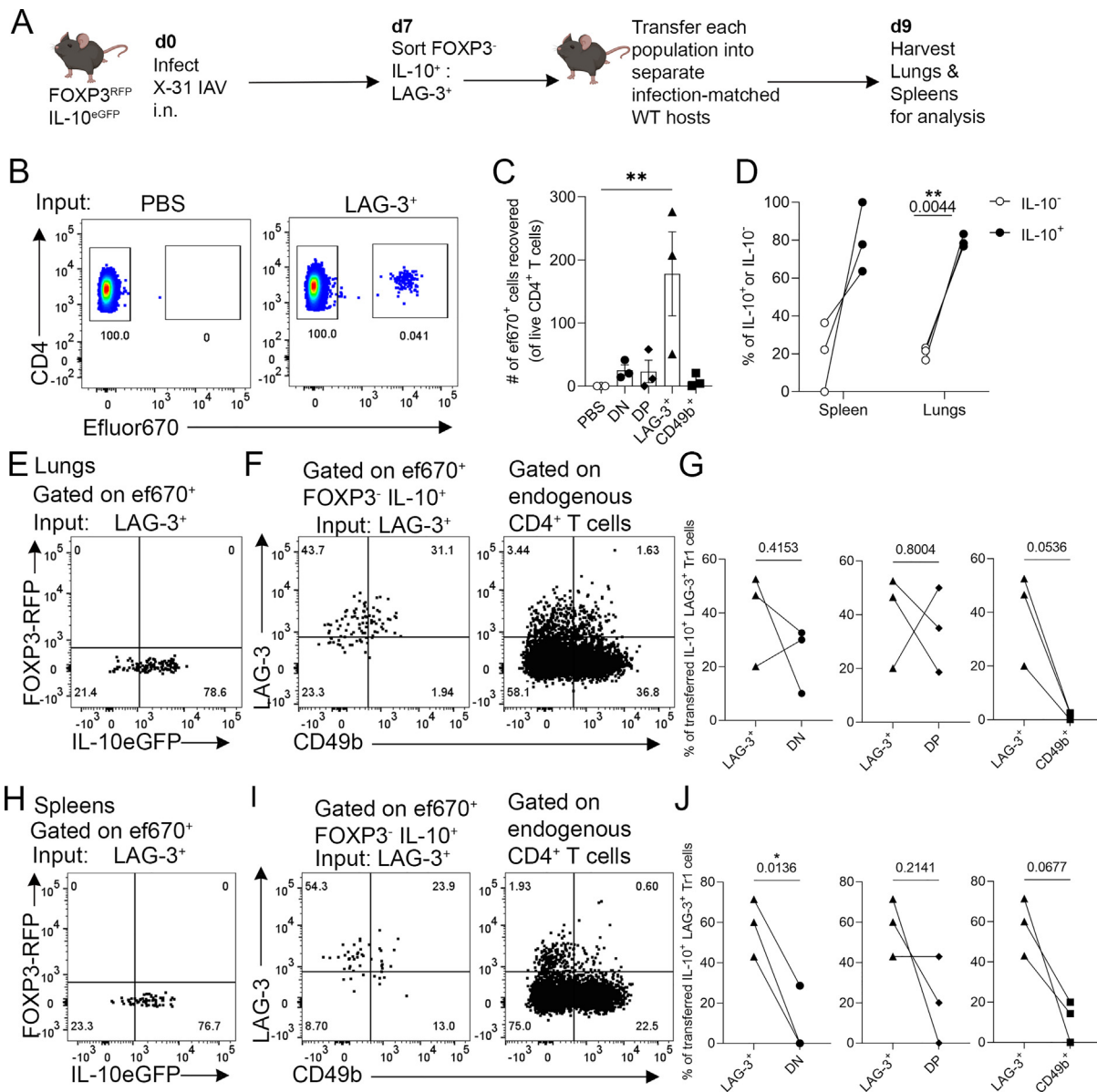


Fig. 8 Plasticity of IAV-induced LAG-3⁺ Tr1 cells from the lung. (A) Experimental schematic. $\text{FOXP3}^{\text{RFP}} \text{IL-10}^{\text{GFP}}$ mice and age-matched C57BL/6 mice were infected with X-31 intranasally. On day 7 post-infection lungs from 3–4 $\text{FOXP3}^{\text{RFP}} \text{IL-10}^{\text{GFP}}$ mice were pooled and Tr1 cells were FACS-sorted (Live, $\text{CD3}^+ \text{CD4}^+ \text{CD44}^+ \text{FOXP3}^- \text{IL-10}^+$) based on expression of LAG-3 and CD49b and transferred intravenously into separate infection-matched hosts. On day 9 post-infection the lungs and spleens were analyzed for Tr1 cell presence and plasticity. (B) Concatenated flow cytometry of Tr1 cell detection in infection-matched lungs (pooled from three independent experiments). (C) The number of ef670⁺ transferred cells recovered from lungs of recipients on day 9 post-infection. (D) The frequency of ef670⁺ transferred cells recovered from spleen and lungs that were LAG-3⁺ and became either IL-10⁻ or remained IL-10⁺. Concatenated (E) lungs and (H) spleens from LAG-3⁺ recipient mice showing transferred LAG-3⁺ Tr1 cell expression of FOXP3 and IL-10. LAG-3 and CD49b expression by input LAG-3⁺ transferred cells that maintain IL-10⁺ (IL-10⁺) (left) and endogenous CD4⁺ T-cells (right) recovered from the (F) lungs and (I) spleen. The frequency of transferred LAG-3⁺ cells recovered from lungs (G) or spleens (J) that remained IL-10⁺ and either maintained LAG-3⁺ or became DN, DP, or CD49b⁺. Data are shown as mean \pm standard error of mean in (C) and as individual paired replicates (D, G, and J), $n = 3$ biological replicates from three independent experiments. Statistical analysis was completed using one-way analysis of variance (C) or multiple paired t tests (D, G, and J) * $p < 0.05$, ** $p < 0.01$. (Fig. made with [Biorender.com](https://www.biorender.com)). CD = clusters of differentiation; DN = double negative; DP = double positive; ef670 = efluor670 proliferation dye; GFP = green fluorescent protein; IAV = influenza A virus; IL = interleukin; LAG-3 = lymphocyte activation gene-3; PBS = phosphate buffered saline; RFP = red fluorescent protein; Tr1 = type I regulatory cell.

persistence of Tr1 cells in the present study substantially differs from that reported in chronic LCMV infection where Tr1 cells continued to accumulate up to day 20⁶⁷, which is in contrast to the abrupt loss of Tr1 cells observed here by day 10 post-

infection. This strict temporal control of Tr1 cells is suggestive of an important window for regulation of the anti-IAV immune response and raises important questions as to the fate and plasticity of these cells in this context.

While the data in this study demonstrate the generation and potential functions of Tr1 cells in acute respiratory virus infection, the fate and persistence of Tr1 cells after response resolution were not fully resolved. Although most Tr1 cells in the lung were lost between day 7 and day 10 post-IAV infection, it was notable that DN Tr1 cells persisted at day 10. On the surface, this initially suggested that DN Tr1 cells may represent an endpoint of Tr1 cell fate in this context. However, transcriptomic analysis instead suggested that DN Tr1 cells were actually the least differentiated Tr1 population (e.g. expressing higher levels of Tfh-like genes such as *Cxcr5*, *Pdcd1*, and *Id3*). This could suggest that the DN population persists as Tfh-like cells that may contribute to B cell responses and iBALT formation in the infected lungs^{68–70}. Furthermore, the CD49b⁺ Tr1 cells were undergoing a higher rate of apoptosis compared to the other populations, suggesting that they are more likely to represent an endpoint of Tr1 cell fate. A potential explanation for these findings is that the DN Tr1 cells observed in this study are a heterogeneous population of IL-10-secreting T cells that contains cells consistent with the definition of Tr1 cells, that have not yet upregulated either CD49b or LAG-3 and also contain cells that have downregulated these markers as they transition to alternative T-cell fates such as Tfh-like cells. These questions could be addressed by developing genetic fate-reporting systems for Tr1 cells such as have been described for Th1, Th2, Treg, and Th17 cells^{71–73}. In support of the concept that Tr1 cells exhibit plasticity *in vivo*, our data indicate that LAG-3⁺ Tr1 cells in acute IAV infection were capable of transitioning to non-Tr1 cells (loss of IL-10 expression) and also to DP and DN Tr1 cells. This suggests that there is substantial plasticity between the observed Tr1 cell populations that emerge during acute IAV infection. Further investigation to untangle this complex web of cellular states using fate-mapping and single-cell approaches is warranted to better understand these key regulatory cells in future.

CONCLUSION

This study provides a thorough investigation into the biology of Tr1 cells in the context of an acute resolving model of infection, with a lack of Tr1 cells correlating with a delay in the resolution of IAV infection in *Il27ra*^{-/-} mice. Four Tr1 cell activation states were delineated based on expression of LAG-3 and/or CD49b. These populations exhibited differences in localization, dependence on IL-10 to suppress T-cell proliferation, and had distinct transcriptional features. LAG-3⁺ Tr1 cells were able to adopt a DN or DP phenotype suggestive of significant plasticity being present between these populations. Overall, a detailed description of Tr1 populations and potential function has been outlined in the present study. This could inform therapeutic efforts to target Treg cells in acute infection to improve patient outcomes.

Limitations of this study

The *Il27ra*^{-/-} mouse was used as a model of Tr1 deficiency. As this is a broad knockout mouse, other IL-27-dependent cell populations may also be affected. To further elucidate the extent of Tr1 contributions to regulation of immune responses other viruses and infection models should be investigated and these should also be examined in human patients during the course of acute respiratory infection.

METHODS

Mice

C57BL/6 FOXP3^{RFP}IL-10^{GFP} (C57BL/6-*Foxp3*^{tm1Flv} × B6.129S6-*Il10*^{tm1Flv})³¹ bred at the University of Adelaide animal house. C57BL/6 *Il27ra*^{-/-} (B6N.129P2-*Il27ra*^{tm1Mak} mice) and genetically matched WT control mice were inter-crossed at the University of Adelaide animal house for littermate experimental mice. C57BL/6J and B6.SJL.*Ptprca* (Ly5.1) mice were purchased from the ARC (Perth, WA). All mice were housed under specific pathogen-free conditions at University of Adelaide Animal Facility. Experiments used gender- and age-matched mice between 8 and 12 weeks of age. Mice were humanely euthanized by CO₂ asphyxiation. All experimental and breeding protocols were approved by the University of Adelaide Animal Ethics Committee under S-2017-040, S-2018-004, S-2019-058, and S-2021-097 ethics approvals.

IAV infection

X-31 and X-31-OVA₃₂₃₋₃₃₉ [H3N2] IAV stocks were grown in 10-day-old embryonated chicken eggs. Each egg was injected with 0.1 ml normal saline containing one hemagglutination unit (HAU) virus, incubated for 48 hours at 37 °C, and held at 4 °C overnight. The amniotic/allantoic fluids were then harvested, pooled, clarified, and stored at -80 °C. These live virus stocks were titrated in Madin-Darby canine kidney cells using a TCID₅₀ assay, and the titres were 2.87 × 10⁶ TCID₅₀/ml for X-31 and 3.13 × 10⁵ TCID₅₀/ml for X-31- OVA₃₂₃₋₃₃₉. For IAV infection, mice were anesthetized with pentobarbitone (Ilium) intra-peritoneally and then i.n. instilled with 923TCID₅₀ (X-31 IAV) or 200TCID₅₀ (X-31-OVA₃₂₃₋₃₃₉) in 32 µl of phosphate buffered saline (PBS). Mice were monitored daily for weight loss. Any mouse reaching >20% of initial weight was humanely euthanized as per institutional animal welfare regulations.

Tissue isolation and processing

For peripheral blood collection, immediately following humane killing, the chest cavity was opened by incisions between ribs. A 29G insulin syringe was used to collect blood by cardiac puncture. The blood was collected into heparinised vacutainer tubes (Becton Dickinson [BD] Biosciences, San Jose, CA, USA). Between 250µL and 500µL of blood was incubated in 10mL mouse red cell lysis buffer (mRCLB) for 20 minutes at 37°C then washed 2-3 times in PBS. Mice were perfused with a 26G needle fitted to a 10mL syringe filled with PBS. The needle was inserted into the left ventricle and a small incision was made in the aorta. For bronchoalveolar lavage collection the trachea was exposed. A superficial incision was made in the trachea just below the nasopharynx. A 1mL syringe was filled with 1mL PBS and fitted with an insyte autoguard catheter (BD Biosciences, San Jose, CA, USA) this was inserted into the tracheal incision orientated towards the lungs. Three washes were performed changing the PBS each time and collecting the fluid. Cells were washed once in PBS, then incubated in 1mL mRCLB for 5min at 37°C before a final two washes in PBS. For lungs, all five lung lobes were harvested and placed into 1mL of lung digestion medium with sodium pyruvate (Dulbecco's modified eagle medium (Gibco/Thermo Fisher Scientific, Grand island, NY, USA) supplemented with 10% FBS (Merk/Sigma-Aldrich, Rahway, NJ, USA), 10mM HEPES (Gibco/Thermo Fisher Scientific, Grand island, NY, USA), 1X penicillin/ streptomycin (Gibco/Thermo Fisher Scientific, Grand island, NY, USA), 2.5mM CaCl₂ and MgCl₂ (Molecular Life Sciences technical services unit, Adelaide, AUS),

30U/mL DNase I (Merk/Sigma-Aldrich, Rahway, NJ, USA), and 1mg/mL Collagenase IA from *Clostridium histolyticum* (Merk/Sigma-Aldrich, Rahway, NJ, USA). Lungs were mechanically minced prior to incubating at 37°C for 30 minutes with shaking and pipetted up and down every 10-15 minutes to ensure homogenisation. The lung suspensions were then passed through 70µm filters (BD Biosciences, San Jose, CA, USA). Spleens and lymph nodes were also prepared by passing through 70µm filters. Lungs, spleens, and lymph nodes were then washed in PBS. Lungs and spleens were then incubated in 5mL mouse red cell lysis buffer for 5-7 minutes at 37°C. Cells were then washed twice in PBS.

Viral load and quantitative polymerase chain reaction

For viral load analysis whole lungs were snap-frozen in liquid nitrogen, ground into fine powder, and resuspended in TRIzol reagent (Invitrogen/Thermo Fisher Scientific, Carlsbad, CA, USA). RNA was then extracted following the manufacturer's protocol. RNA samples were DNase treated using Turbo DNA-free kit (Invitrogen/Thermo Fisher Scientific, Carlsbad, CA, USA), prior to cDNA synthesis (High-Capacity cDNA synthesis kit, Applied Biosystems/Thermo Fisher Scientific Baltics, UAB). Quantitative reverse transcription-polymerase chain reaction was conducted using LightCycler-480 SYBR Green I Power-Up Master Mix (Applied Biosystems/Thermo Fisher Scientific Baltics, UAB) on a LightCycler-480 instrument (Roche, Rotkreuz, Switzerland). Relative expression was calculated by normalizing to mouse *Rplp0* as previously described using the $2^{-\Delta C_p}$ method⁷⁴. All polymerase chain reaction primers used are listed in [Supplementary Table 1](#).

Flow cytometry, cell sorting, and antibodies

Single-cell suspensions were stained in 96 well round-bottom plates (Sigma-Aldrich/Corning, Saint Louis, MO, USA) at 2×10^6 lymphocytes per well with antibodies and other reagents detailed in [Supplementary Table 2](#). Cells were washed once in PBS then resuspended in fixable viability stain 780 (BD Biosciences, San Jose, CA, USA) diluted 1/1000 in PBS and blocked with mouse γ -globulin (Rockland, Bedford, Pennsylvania, USA) at 10 µg/ml for 5 minutes at room temperature in the dark. Cells were stained with directly conjugated and biotinylated antibodies diluted in FACS buffer or Brilliant Stain Buffer (BD Biosciences, San Jose, CA, USA) for 20 minutes at 4 °C, with the exception of anti-mouse CD49b (HMa2, BD Biosciences, San Jose, CA, USA) and anti-mouse LAG-3 (C9B7W, Biolegend, San Diego, CA, USA), which were stained for 60 minutes at 37 °C as previously described^{23,27}. For co-staining FOXP3 and IL-10 in WT mice, 2×10^6 cells/well were restimulated with 10 µg/ml plate bound α CD3 (145-2C11, BioXcell, Lebanon, NH, USA) and 1 µg/ml soluble α CD28 (37.51, BD Biosciences, San Jose, CA, USA) and incubated at 37 °C and 5% CO₂. After 2 hours, 20 µl of a solution containing 10 µg/ml of Brefeldin A (eBioscience/Thermo Fisher Scientific, Carlsbad, CA, USA) and 10 µM Monensin (BD Biosciences, San Jose, CA, USA) in complete iscove's modified dulbecco's (IMDM) were added and mixed gently before incubation for a further 4 hours at 37 °C and 5% CO₂. After restimulation, cells were transferred to a new plate for staining. Stained cells were analyzed using a BD Fortessa X20 cytometer (BD Biosciences, San Jose, CA, USA) at the University of Adelaide or sorted using a BD FACSAriaIIImu (BD Biosciences, San Jose, CA, USA) or a BD FACSAria Fusion (BD Biosciences, San Jose, CA, USA) at The University of Adelaide or SAHMRI.

In vitro suppression assays

5×10^3 CD11c-enriched APCs were used in each well of the assay, obtained from naïve C57BL/6 spleens using a CD11c positive isolation kit (StemCell, Vancouver, BC, Canada). Soluble α CD3 (145-2C11, 1 µg/ml, BioXcell, Lebanon, NH, USA) was added on top. Responding T cells were isolated from spleens and inguinal lymph nodes of naïve Ly5.1 mice using a pan naïve CD3⁺ negative selection kit (StemCell, Vancouver, BC, Canada) and then FACS-sorted (viable, CD3⁺CD25⁻) to achieve >95% purity and labeled with Efluor670 proliferation dye (ebioscience/Thermo Fisher Scientific, Carlsbad, CA, USA). Tr1 cells were FACS-sorted (viable CD3⁺CD4⁺CD44⁺FOXP3⁻IL-10⁺, separated into four populations based on co-expression of LAG-3 and CD49b) from IAV-infected FOXP3^{RFP}IL-10^{GFP} mouse lungs on day 7 post-infection. 2×10^4 Tr1 cells were co-cultured with 2×10^4 labeled T cells for a 1:1 effector:Tr1 ratio. Tregs derived from secondary lymphoid organs were used as a positive control to establish high levels of suppression in these assays ([Fig. 5](#)). Negative controls to set a threshold for genuine suppression in this assay were also included. To assess the background in this assay due to competition for stimulation and not due to suppressive function of the added cells, effector cells were co-cultured with effector cells (at a 1:1 ratio). Suppression assays were analyzed using the proliferation modeling function in FlowJo™ v10.8 software (Treestar, Ashland, OR, USA) and % suppression was calculated using the following formula: $100 \times (1 - DI_{Tr1} / DI_{eff})$ based on division index (DI) as described previously^{75,76}.

Intravascular labeling

Three µg of α TCR- β -BV421 (H57-597, Biolegend, San Diego, CA, USA) was diluted in 200 µL of Dulbecco's phosphate buffered saline (dPBS) (Merk/Sigma-Aldrich, Rahway, NJ, USA) per mouse, which was injected intravenously 3 minutes prior to humane euthanasia as previously described⁷⁷.

Adoptive transfer of Tr1 cells into IAV infection-matched hosts

FOXP3^{RFP}IL-10^{GFP} and C57BL/6 mice were infected i.n. with X-31 IAV. On day 7 post-infection, single-cell suspensions were prepared from infected lungs from FOXP3^{RFP}IL-10^{GFP} mice and cells labeled with efluor670 dye (ebioscience/Thermo Fisher Scientific, Carlsbad, CA, USA). Tr1 cells were then FACS-sorted (live CD3⁺CD4⁺CD44⁺FOXP3^{RFP}IL-10^{GFP+} separated into four populations based on co-expression of LAG-3 and CD49b). Infection-matched C57BL/6 mice received intravenous injection of Tr1 cells or dPBS vehicle. On day 9 post-infection, recipients were humanely euthanized and tissues harvested to quantify transferred Tr1 cells and assess plasticity.

RNA sequencing

For sequencing, lung cells were isolated and stained and Tr1 cell populations were FACS-sorted using a FACSAriaIIImu. Total RNA was extracted using a Arcturus Pico Pure RNA Extraction kit (Applied Biosystems/Thermo Fisher Scientific, Carlsbad, CA, USA) following the manufacturer's protocol. DNA digestion was performed using an RNase-free DNase kit (Qiagen, Aarhus, Denmark). Total RNA was eluted in 20 µl elution buffer. RNA sequencing of 150 bp paired-end reads at an average of 30 M reads per sample was performed by Novogene. Data quality control (QC) for the RNA sequencing experiment was conducted using FastQC⁷⁸ and ngsReports⁷⁹. Read trimming and filtering

were performed using AdapterRemoval v2.2.1⁸⁰, with reads aligned to GRCm38 using STARv2.5.3⁸¹. Reads were summarized to gene-level counts using featureCounts and gene annotations provided by Ensembl Release 96. Differential Expression analysis was performed using voom⁸² with sample-level quality weights assigned by nesting the four cell lines within each mouse. AFDR-adjusted p value < 0.05 along with an estimated log Fold-Change (LFC) beyond the range ± 1 was used to consider a gene as DE, Enrichment testing was performed using ClusterProfiler⁸³, taking all detectable genes as the universe against which to test for enrichment. Mapping from gene to Gene Ontology was obtained using the Bioconductor package org.Mm.eg.db, and a Bonferroni-adjusted p value < 0.05 was used to consider an ontology enriched in any of the sets of DE genes⁸⁴. An UpSet plot was generated from a complete list of DE genes after filtering by FDR and LFC. For this comparison, any genes with an FDR-adjusted p value < 0.05 was considered significant in this analysis to give a comprehensive result and define population-specific signature genes. All analytic code is available via GitHub (<https://caitlinabbott.github.io/Tr1-RNA-Sequencing/>).

Statistical Analysis

All statistical analysis aside from the RNA sequencing experiment was performed using GraphPad Prism software v9 for windows (GraphPad Software, San Diego, California USA, www.graphpad.com). Statistical tests are detailed in the figure legends.

AUTHOR CONTRIBUTIONS

CA conceptualized the project performed experiments and wrote the manuscript. CA, TT, TN, and IC designed experiments. EF and TT performed experiments. MA, SP, TT, TN, and GH provided important intellectual input and edited the manuscript. SP provided critical expertise with the RNA sequencing data set and generated the online repository. ZQ and MA³ assisted with the RNA sequencing analysis. IC and SM supervised the study, sourced and provided funding for the project, and wrote the manuscript. All authors contributed to the final article.

DECLARATIONS OF COMPETING INTEREST

The authors have no competing interests to declare.

FUNDING

This research was supported by National Health and Medical Research Council project and ideas grants 1163335 and 2019024 held by SRM, IC, and MA². CA, EF, TT, and TN were supported by Research Training Program Scholarships. IC is supported by a Senior Fellowship from Multiple Sclerosis Australia.

ACKNOWLEDGMENTS

We would like to thank all staff at laboratory animal services at the University of Adelaide for assistance with animal husbandry, Dr. Randall Grose at South Australian Health and Medical Research Institute for assistance with cell sorting, Professor Stephen Turner (Monash University) for providing the X-31-OVA₃₂₃₋₃₃₉ influenza A virus, and Professor Christian Engwerda (QIMR) for providing interleukin-27ra^{-/-} mice.

APPENDIX A. SUPPLEMENTARY DATA

Supplementary data to this article can be found online at <https://doi.org/10.1016/j.mucimm.2023.06.003>.

REFERENCES

- Ruckwardt, T. J., Bonaparte, K. L., Nason, M. C. & Graham, B. S. Regulatory T cells promote early influx of CD8+ T cells in the lungs of respiratory syncytial virus-infected mice and diminish immunodominance disparities. *J. Virol.* **83**, 3019–3028 (2009).
- Sehrawat, S., Suvas, S., Sarangi, P. P., Suryawanshi, A. & Rouse, B. T. In vitro-generated antigen-specific CD4+ CD25+ Foxp3+ regulatory T cells control the severity of herpes simplex virus-induced ocular immunoinflammatory lesions. *J. Virol.* **82**, 6838–6851 (2008).
- Rogers, M. C. et al. CD4+ regulatory T cells exert differential functions during early and late stages of the immune response to respiratory viruses. *J. Immunol.* **201**, 1253–1266 (2018).
- Lund, J. M., Hsing, L., Pham, T. T. & Rudensky, A. Y. Coordination of early protective immunity to viral infection by regulatory T cells. *Science* **320**, 1220–1224 (2008).
- Fulton, R. B., Meyerholz, D. K. & Varga, S. M. Foxp3+ CD4 regulatory T cells limit pulmonary immunopathology by modulating the CD8 T cell response during respiratory syncytial virus infection. *J. Immunol.* **185**, 2382–2392 (2010).
- Zou, Q. et al. CD8+ Treg cells suppress CD8+ T cell-responses by IL-10-dependent mechanism during H5N1 influenza virus infection. *Eur. J. Immunol.* **44**, 103–114 (2014).
- Lu, C. et al. Memory regulatory T cells home to the lung and control influenza A virus infection. *Immunol. Cell Biol.* **97**, 774–786 (2019).
- Arpaia, N. et al. A distinct function of regulatory T cells in tissue protection. *Cell* **162**, 1078–1089 (2015).
- Roncarolo, M. G. et al. Autoreactive T cell clones specific for class I and class II HLA antigens isolated from a human chimera. *J. Exp. Med.* **167**, 1523–1534 (1988).
- Bacchetta, R. et al. Host-reactive CD4+ and CD8+ T cell clones isolated from a human chimera produce IL-5, IL-2, IFN-gamma and granulocyte/macrophage-colony-stimulating factor but not IL-4. *J. Immunol.* **144**, 902–908 (1990).
- Groux, H. et al. A CD4+ T-cell subset inhibits antigen-specific T-cell responses and prevents colitis. *Nature* **389**, 737–742 (1997).
- Heinzel, F. P., Sadick, M. D., Mutha, S. S. & Locksley, R. M. Production of interferon gamma, interleukin 2, interleukin 4, and interleukin 10 by CD4+ lymphocytes in vivo during healing and progressive murine leishmaniasis. *PNAS* **88**, 7011–7015 (1991).
- Ghalib, H. W. et al. Interleukin 10 production correlates with pathology in human Leishmania donovani infections. *J. Clin. Invest.* **92**, 324–329 (1993).
- Holaday, B. J. et al. Potential role for interleukin-10 in the immunosuppression associated with Kala Azar. *J. Clin. Invest.* **92**, 2626–2632 (1993).
- Reiner, S. L., Zheng, S., Wang, Z. E., Stowring, L. & Locksley, R. M. Leishmania promastigotes evade interleukin 12 (IL-12) induction by macrophages and stimulate a broad range of cytokines from CD4+ T cells during initiation of infection. *J. Exp. Med.* **179**, 447–456 (1994).
- Reed, S. G. et al. IL-10 mediates susceptibility to Trypanosoma cruzi infection. *J. Immunol.* **153**, 3135–3140 (1994).
- Hagenbaugh, A. et al. Altered immune responses in interleukin 10 transgenic mice. *J. Exp. Med.* **185**, 2101–2110 (1997).
- Roncarolo, M. G., Gregori, S., Bacchetta, R., Battaglia, M. & Gagliani, N. The biology of T regulatory type 1 cells and their therapeutic application in immune-mediated diseases. *Immunity* **49**, 1004–1019 (2018).
- Pot, C. et al. Cutting edge: IL-27 induces the transcription factor c-Maf, cytokine IL-21, and the costimulatory receptor ICOS that coordinately act together to promote differentiation of IL-10-producing Tr1 cells. *J. Immunol.* **183**, 797–801 (2009).
- Batten, M. et al. Cutting edge: IL-27 is a potent inducer of IL-10 but not FoxP3 in murine T cells. *J. Immunol.* **180**, 2752–2756 (2008).
- Zhang, H. et al. An IL-27-driven transcriptional network identifies regulators of IL-10 expression across T helper cell subsets. *Cell Rep.* **33**:108433.
- Gagliani, N., Vesely, M. C. A. & Iseppon, A., et al. TH17 cells transdifferentiate into regulatory T cells during resolution of inflammation. *Nature* **523**, 221–225 (2015).
- Brockmann, L. et al. Molecular and functional heterogeneity of IL-10-producing CD4+ T cells. *Nat. Commun.* **9**, 5457 (2018).
- Akdis, M. et al. Immune responses in healthy and allergic individuals are characterized by a fine balance between allergen-specific T regulatory 1 and T helper 2 cells. *J. Exp. Med.* **199**, 1567–1575 (2004).
- Meiler, F. & Zumbkehr, J., et al. In vivo switch to IL-10-secreting T regulatory cells in high dose allergen exposure. *J. Exp. Med.* **205**, 2887–2898 (2008).
- Huang, W., Solouki, S., Koylass, N., Zhengv, S. G. & August, A. ITK signalling via the Ras/IRF4 pathway regulates the development and function of Tr1 cells. *Nat. Commun.* **8**, 15871 (2017).

27. Gagliani, N., Magnani, C. & Huber, S., et al. Coexpression of CD49b and LAG-3 identifies human and mouse T regulatory type 1 cells. *Nat. Med.* **19**, 739–746 (2013).
28. Montes de Oca, M. et al. Blimp-1-Dependent IL-10 production by Tr1 cells regulates TNF-mediated tissue pathology. *PLoS Pathog.* **12**, e1005398 (2016).
29. Yu, H. et al. Intestinal type 1 regulatory T cells migrate to periphery to suppress diabetogenic T cells and prevent diabetes development. *PNAS* **114**, 10443–10448 (2017).
30. Karwacz, K., Miraldi, E. & Pokrovskii, M., et al. Critical role of IRF1 and BATF in forming chromatin landscape during type 1 regulatory cell differentiation. *Nat. Immunol.* **18**, 412–421 (2017).
31. Zhang, P. et al. Eomesodermin promotes the development of type 1 regulatory T (TR1) cells. *Sci. Immunol.* **2**, eaah7152 (2017).
32. Sun, J., Madan, R., Karp, C. L. & Braciale, T. J. Effector T cells control lung inflammation during acute influenza virus infection by producing IL-10. *Nat. Med.* **15**, 277–284 (2009).
33. Kretschmer, U. et al. Expression of selectin ligands on murine effector and IL-10-producing CD4+ T cells from non-infected and infected tissues. *Eur. J. Immunol.* **34**, 3070–3081 (2004).
34. Kimball, A. B. et al. Clinical and immunologic assessment of patients with psoriasis in a randomized, double-blind, placebo-controlled trial using recombinant human interleukin 10. *Arch. Dermatol.* **138**, 1341–1346 (2002).
35. Kanai, K. et al. Murine γ -herpesvirus 68 induces severe lung inflammation in IL-27-deficient mice with liver dysfunction preventable by oral neomycin. *J. Immunol.* **200**, 2703–2713 (2018).
36. Thelen, B. et al. Eomes is sufficient to regulate IL-10 expression and cytotoxic effector molecules in murine CD4+ T cells. *Front. Immunol.* **14**, 1058267 (2023).
37. Sun, J. et al. Autocrine regulation of pulmonary inflammation by effector T-cell derived IL-10 during infection with respiratory syncytial virus. *PLoS Pathog.* **7**, e1002173 (2011).
38. Weiss, K. A., Christiaansen, A. F., Fulton, R. B., Meyerholz, D. K. & Varga, S. M. Multiple CD4+ T cell subsets produce immunomodulatory IL-10 during respiratory syncytial virus infection. *J. Immunol.* **187**, 3145–3154 (2011).
39. Pyle, C. J., Uwadiae, F. I., Swieboda, D. P. & Harker, J. A. Early IL-6 signalling promotes IL-27 dependent maturation of regulatory T cells in the lungs and resolution of viral immunopathology. *PLoS Pathog.* **13**, e1006640 (2017).
40. Wan, Y. Y. & Flavell, R. A. Identifying Foxp3-expressing suppressor T cells with a bicistronic reporter. *PNAS* **102**, 5126–5131 (2005).
41. Kamanaka, M. & Kim, S. T., et al. Expression of interleukin-10 in intestinal lymphocytes detected by an interleukin-10 reporter knockin tiger mouse. *Immunity* **25**, 941–952 (2006).
42. Morishima, N. et al. Augmentation of effector CD8+ T cell generation with enhanced granzyme B expression by IL-27. *J. Immunol.* **175**, 1686–1693 (2005).
43. Harker, J. A. et al. Interleukin-27R signaling mediates early viral containment and impacts innate and adaptive immunity after chronic lymphocytic choriomeningitis virus infection. *J. Virol.* **92**:e02196-17.
44. Matsui, M. et al. Interleukin-27 activates natural killer cells and suppresses NK-resistant head and neck squamous cell carcinoma through inducing antibody-dependent cellular cytotoxicity. *Cancer Res.* **69**, 2523–2530 (2009).
45. Yao, Y. et al. Tr1 cells, but not Foxp3+ regulatory T cells, suppress NLRP3 inflammasome activation via an IL-10–dependent mechanism. *J. Immunol.* **195**, 488–497 (2015).
46. Cook, L. et al. Suppressive and gut-reparative functions of human Type 1 T regulatory cells. *Gastroenterology* **157**, 1584–1598 (2019).
47. Lawrence, C. W., Ream, R. M. & Braciale, T. J. Frequency, specificity, and sites of expansion of CD8+ T cells during primary pulmonary influenza virus infection. *J. Immunol.* **174**, 5332–5340 (2005).
48. Flynn, K. J. et al. Virus-specific CD8+ T cells in primary and secondary influenza pneumonia. *Immunity* **8**, 683–691 (1998).
49. Belz, G. T., Xie, W. & Doherty, P. C. Diversity of epitope and cytokine profiles for primary and secondary influenza A virus-specific CD8+ T cell Responses¹. *J. Immunol.* **166**, 4627–4633 (2001).
50. Levings, M. K., Sangregorio, R. & Roncarolo, M. G. Human Cd25(+)/CD4(+)-T regulatory cells suppress naive and memory T cell proliferation and can be expanded in vitro without loss of function. *J. Exp. Med.* **193**, 1295–1302 (2001).
51. Brockmann, L. & Gagliani, N., et al. IL-10 receptor signaling is essential for T_R1 cell function in vivo. *J. Immunol.* **198**, 1130–1141 (2017).
52. Gregori, S. et al. Differentiation of type 1 T regulatory cells (Tr1) by tolerogenic DC-10 requires the IL-10–dependent ILT4/HLA-G pathway. *Blood* **116**, 935–944 (2010).
53. Agata, Y. et al. Expression of the PD-1 antigen on the surface of stimulated mouse T and B lymphocytes. *Int. Immunol.* **8**, 765–772 (1996).
54. Tocheva, A. S. et al. Quantitative phosphoproteomic analysis reveals involvement of PD-1 in multiple T cell functions. *J. Biol. Chem.* **295**, 18036–18050 (2020).
55. Hastings, W. D. et al. TIM-3 is expressed on activated human CD4+ T cells and regulates Th1 and Th17 cytokines. *Eur. J. Immunol.* **39**, 2492–2501 (2009).
56. Vieira, P. L. et al. IL-10-secreting regulatory T cells do not express Foxp3 but have comparable regulatory function to naturally occurring CD4+CD25+ regulatory T cells. *J. Immunol.* **172**, 5986–5993 (2004).
57. Chen, P. P. et al. Alloantigen-specific type 1 regulatory T cells suppress through CTLA-4 and PD-1 pathways and persist long-term in patients. *Sci. Transl. Med.* **13**, eabf5264 (2021).
58. Di Virgilio, F., Dal Ben, D., Sarti, A. C., Giuliani, A. L. & Falzoni, S. The P2X7 receptor in infection and inflammation. *Immunity* **47**, 15–31 (2017).
59. Borges da Silva, H. et al. The purinergic receptor P2RX7 directs metabolic fitness of long-lived memory CD8+ T cells. *Nature* **559**, 264–268 (2018).
60. Jankovic, D. et al. Conventional T-bet(+)/Foxp3(–) Th1 cells are the major source of host-protective regulatory IL-10 during intracellular protozoan infection. *J. Exp. Med.* **204**, 273–283 (2007).
61. Neumann, C. et al. Role of Blimp-1 in programming Th effector cells into IL-10 producers. *J. Exp. Med.* **211**, 1807–1819 (2014).
62. Roers, A. et al. T cell–specific inactivation of the interleukin 10 gene in mice results in enhanced T cell responses but normal innate responses to lipopolysaccharide or skin irritation. *J. Exp. Med.* **200**, 1289–1297 (2004).
63. Bedke, T. & Iannitti, R. G., et al. Distinct and complementary roles for *Aspergillus fumigatus*-specific Tr1 and Foxp3+ regulatory T cells in humans and mice. *Immunol. Cell Biol.* **92**, 659–670 (2014).
64. Cavani, A. et al. Human CD4+ T lymphocytes with remarkable regulatory functions on dendritic cells and nickel-specific Th1 immune responses. *J. Invest. Dermatol.* **114**, 295–302 (2000).
65. Brincks, E. L. et al. Antigen-specific memory regulatory CD4+Foxp3+ T cells control memory responses to influenza virus infection. *J. Immunol.* **190**, 3438–3446 (2013).
66. Huber, S., Gagliani, N. & Esplugues, E., et al. Th17 cells express interleukin-10 receptor and are controlled by Foxp3[–] and Foxp3⁺ regulatory CD4+ T cells in an interleukin-10-dependent manner. *Immunity* **34**, 554–565 (2011).
67. Parish, I. A. et al. Chronic viral infection promotes sustained Th1-derived immunoregulatory IL-10 via BLIMP-1. *J. Clin. Invest.* **124**, 3455–3468 (2014).
68. Solé, P. et al. A T follicular helper cell origin for T regulatory type 1 cells. *Cell. Mol. Immunol.* **20**, 489–511 (2023).
69. Cañete, P. F. et al. Regulatory roles of IL-10–producing human follicular T cells. *J. Exp. Med.* **216**, 1843–1856 (2019).
70. Moyron-Quiroz, J. E. et al. Role of inducible bronchus associated lymphoid tissue (iBALT) in respiratory immunity. *Nat. Med.* **10**, 927–934 (2004).
71. Croxford, A. L., Kurschus, F. C. & Waisman, A. Cutting edge: an IL-17-CreEYFP reporter mouse allows fate mapping of Th17 cells. *J. Immunol.* **182**, 1237–1241 (2009).
72. Lee, S. E., Rudd, B. D. & Smith, N. L. Fate-mapping mice: new tools and technology for immune discovery. *Trends Immunol.* **43**, 195–209 (2022).
73. Rubtsov, Y. P. & Niec, R. E., et al. Stability of the regulatory T cell lineage in vivo. *Science* **329**, 1667–1671 (2010).
74. Schmittgen, T. D. & Livak, K. J. Analyzing real-time PCR data by the comparative C(T) method. *Nat. Protoc.* **3**, 1101–1108 (2008).
75. Collison, L. W. & Vignali, D. A. A. In vitro Treg suppression assays. *Methods Mol. Biol.* **707**, 21–37 (2011).
76. Ward, S. T., Li, K. K. & Curbishley, S. M. A method for conducting suppression assays using small numbers of tissue-isolated regulatory T cells. *MethodsX* **1**, 168–174 (2014).
77. Anderson, K. G. et al. Intravascular staining for discrimination of vascular and tissue leukocytes. *Nat. Protoc.* **9**, 209–222 (2014).
78. Andrews, S. Babraham Bioinformatics - FastQC A Quality Control tool for High Throughput Sequence Data. Babraham Bioinforma. Available at: <https://www.bioinformatics.babraham.ac.uk/projects/fastqc/> (2019) [Date accessed: 15 November 2022].
79. Ward, C. M., To, T. H. & Pederson, S. M. ngsReports: a Bioconductor package for managing FastQC reports and other NGS related log files. *Bioinformatics* **36**, 2587–2588 (2020).
80. Schubert, M., Lindgreen, S. & Orlando, L. AdapterRemoval v2: rapid adapter trimming, identification, and read merging. *BMC. Res. Notes* **9**, 88 (2016).
81. Dobin, A. et al. STAR: ultrafast universal RNA-seq aligner. *Bioinformatics* **29**, 15–21 (2013).
82. Law, C. W., Chen, Y., Shi, W. & Smyth, G. K. voom: precision weights unlock linear model analysis tools for RNA-seq read counts. *Genome Biol.* **15**, R29 (2014).
83. Yu, G., Wang, L. G., Han, Y. & He, Q. Y. clusterProfiler: an R package for comparing biological themes among gene clusters. *OMICS* **16**, 284–287 (2012).
84. Kolde, R. Pheatmap: pretty heatmaps. R package version 2012. 1, 726 (2018).